



**Arab Academy for Science, Technology & Maritime Transport
College of Engineering & Technology
Construction & Building Department**

Abstract of the M.Sc. Thesis submitted by:

Hassan Ahmed Hassan Ahmed Saad

Title of Thesis:

Effect of Environmental Corrosion on Sea Front Reinforced Concrete Structures

Supervisors: **Ass. Prof. Abdel Moneim Yaseen Sanad**

Dr. Maged Abdel Ghafaar Moussa

Registration date: September 2010

Examination date: July 2013

ABSTRACT

Corrosion of reinforcement steel is a major factor affecting the deterioration of reinforced concrete structures. During corrosion, steel undergoes several phases of chemical reactions with consequent variation in steel section geometry and mechanical properties. At ultimate corrosion stage, the effective cross section area of steel is reduced with equivalent decrease in load carrying capacity leading to unsafe structures. During initial phase of corrosion, chemical reactions generate new products which irregularly increase steel bar diameters. The resulted products induce additional stresses on the structural member, causing cracking and spalling of the concrete cover, and subsequently faster deteriorate the member strength.

Concrete is a durable material, much more than steel and the encasement of steel in it provides the steel with a protective environment and allows it to function effectively as reinforcement. Durability of concrete structures is considered as implicitly acquired as long as the concrete strength satisfies the required design limitation. Bond between reinforcement and concrete is necessary to ensure composite action of the two materials. Testing for bond strength is carried out in variety of ways: standard pull-out, beam anchorage, beam end, and splice tests. The most common and

traditional method is the standard pull-out test and this is the type used in this research.

Rapid deterioration of reinforced concrete buildings in Alexandria, Egypt has become a major problem for sea front buildings' dwellers. Many evidences of deteriorations have been collected, evaluated and some of them have been practically tested. The effect of steel corrosion on durability of sea front reinforced concrete structures is currently investigated using a comprehensive experimental program and detailed numerical analysis at the Arab Academy. The corrosion of different types of carbon steel bars has been evaluated for; Plain bars, un-coated deformed bars and epoxy coated deformed bars. Numerically, a two dimensional finite element model was developed to study the crack initiation and propagation in concrete using nonlinear analysis and specific properties for both steel and concrete elements.

STATEMENT

This dissertation is submitted to the Construction and Building Department, College of Engineering, Arab Academy for Science, Technology & Maritime Transport, for the degree of Master of Science in Construction & Building Engineering.

The work included in this dissertation was carried out by the author in the Construction & Building Department, College of Engineering, Arab Academy for Science, Technology & Maritime Transport from September 2010 to July 2013.

No part of this dissertation has been submitted to any other university or institute for the award of a degree or a qualification.

Author's Name: Hassan Ahmed Hassan Ahmed saad

Signature:

Date: 03 / 07 / 2013

ACKNOWLEDGEMENT

First ALLAH is praised for the aid and guidance.

The present work was conducted out at the Construction & Building Department, College of Engineering & Technology, Arab Academy for Science & Technology, Cairo, Egypt.

The author would like to express his deepest gratitude and appreciation to his supervisors Dr. Abdel Moneim Sanad and Dr. Maged Abdel Ghafaar for their continuous advises through the whole research. Their support and valuable remarks were greatly useful and helpful to achieve effective and beneficial results.

The experimental work was carried out at the Arab Academy for Science & Technology, Cairo, Egypt. The great help of the Construction and Building department and the materials laboratory technician “Soliman Mohye” is highly appreciated.

Special thanks for the helpful academic colleagues (Teaching assistants and undergraduate students) for their helpful advice in contributing to the development of this research. Special thanks for Engineers (Dalia, El-Sayad, Mostafa, Abdel Aal, and Al-Baraa).

The author would like to send his worm and sincere thanks to his father “Eng. Ahmed Hassan” for his valuable support, assistance, and endless help throughout all stages of the research; including but not limited to: materials supply and preparation. This work would have been insurmountable without his hard work, knowledge and editing skills.

Last, the author would like to express his deep feelings towards each member of his family to whom he owes every success in his life. His cordial thanks spread out to his mother, father, sister, and brother for their love, support and guidance throughout his life and for inculcating in him the passion for knowledge.

Hassan Ahmed
July 2013

TABLE OF CONTENTS

ABSTRACT.....	ii
ACKNOWLEDGEMENTS.....	v
LIST OF TABLES.....	x
LIST OF FIGURES.....	xiii
CHAPTER 1 INTRODUCTION.....	1
1.1 General.....	1
1.2 Scope and Objectives.....	8
1.3 Thesis Structure.....	8
CHAPTER 2 THE BOND MECHANISM.....	11
2.1 Introduction.....	11
2.2 Bond between Reinforcing Steel and Concrete.....	11
2.2.1 Chemical Adhesion.....	12
2.2.2 Friction.....	12
2.2.3 Mechanical Interlock.....	12
2.3 Factors Affecting Concrete Rebar Bond Strength.....	15
2.3.1 Geometry and Shape.....	15
2.3.2 Rib Angle.....	16
2.3.3 Rib Spacing and Rib Height.....	17
2.3.4 Casting Position and Concrete Confinement.....	24
2.3.5 Concrete Cover and Bar Spacing.....	27
2.3.6 Development and Splice Length.....	27
2.3.7 Steel Stress and Yield Stress.....	28
2.3.8 Aggregate Type and Quantity.....	29
2.4 Bond Failure Modes.....	29
2.4.1 Un-Cracked Stage.....	30
2.4.2 Micro-Cracks.....	30
2.4.3 Splitting Cracks.....	31
2.4.4 Bond Failure of Plain Bars.....	32
2.4.5 Bond Failure of Deformed Bars Surrounded By Light Confinement.....	32
2.4.6 Bond Failure of Deformed Bars Surrounded By Heavy Confinement.....	33
2.4.7 The ACI Committee 408 Failure Modes.....	34
CHAPTER 3 MECHANISMS OF STEEL CORROSION.....	35
3.1 Introduction.....	35
3.2 Passivation Oxide Films on Iron.....	36
3.3 Depassivation of Steel.....	37
3.4 Corrosion Initiation on Iron and Steel.....	39
3.5 Critical Chloride Content.....	41

3.6	Types of Corrosion.....	45
3.6.1	Dry Corrosion.....	47
3.6.2	Wet Corrosion.....	47
3.7	Corrosion Stages.....	47
3.8	Factors Affecting Corrosion and its Rate.....	49
3.8.1	Factors Related to Concrete.....	49
3.8.1.1	Permeability.....	49
3.8.1.2	Diffusivity.....	50
3.8.1.3	Sorptivity.....	51
3.8.1.4	Water/Cement Ratio and Curing.....	51
3.8.1.5	Concrete Cover Thickness.....	53
3.8.2	Factors Related to the Surrounding Environment.....	56
3.8.2.1	Atmospheric Zone.....	57
3.8.2.2	Tidal Zone.....	58
3.8.2.3	Submerged Zone.....	59
3.9	Chloride Resistance of Concrete.....	59
3.10	Corrosion Rate Calculation.....	62
3.11	Corrosion Monitoring.....	69
3.11.1	Open Circuit Potential (OCP) Measurement.....	70
3.11.2	Surface Potential (SP) Measurement.....	70
3.11.3	Concrete Resistivity Measurement.....	72
3.11.4	Linear Polarization Resistance (LPR) Measurement.....	73
3.11.5	Embeddable Corrosion Monitoring Sensor.....	74
3.11.6	Cover Thickness Measurement.....	74
3.11.7	Ultrasonic Pulse Velocity Technique.....	75
3.11.8	X-ray / Gamma Radiography.....	77
3.11.9	Visual Inspection.....	77
 CHAPTER 4 BOND PERFORMANCE IN DIFFERENT CONCRETE AND STEEL TYPES.....		 78
4.1	High Performance Concrete (HPC).....	78
4.1.1	Supplementary Cementing Materials (SCM).....	79
4.1.2	Silica Fume Concrete.....	80
4.1.3	Fly Ash Concrete.....	83
4.2	Methods of Bond Testing.....	85
4.2.1	Standard Pull-Out Test.....	86
4.2.2	Beam Anchorage Test.....	86
4.2.3	Beam End Test.....	87
4.2.4	Splice Test.....	87
4.3	Effect of Silica Fume Concrete on Bond Stress.....	88
4.4	Effect of Fly Ash Concrete on Bond Stress.....	91
4.5	Performance of Bond for Epoxy Coated Bars.....	95
4.6	Performance of Bond for Corroded Bars.....	105
 CHAPTER 5 METHODS FOR REINFORCEMENT CORROSION ELIMINATION.....		 110
5.1	Carbon Steels Reinforcing Bars.....	110
5.2	Protective Coatings.....	113

5.2.1	Metallic Coatings.....	113
5.2.1.1	Aluminum Coating.....	114
5.2.1.2	Cadmium Coating.....	114
5.2.1.3	Chromium Coating.....	114
5.2.1.4	Nickel Coating.....	115
5.2.1.5	Zinc Coating.....	115
5.2.2	Inorganic Coatings.....	116
5.2.3	Organic Coatings.....	118
5.2.4	Field Performance of Epoxy-Coated Reinforcing Steel.....	118
5.3	Corrosion Inhibitors.....	124
5.3.1	Inhibitors' Classification.....	125
5.3.2	Concrete Reinforcement Corrosion Inhibitors.....	128
5.4	Cathodic Protection.....	129
5.4.1	Theoretical Basis.....	130
5.4.2	Cathodic Protection of Reinforced Concrete Structures.....	131
5.4.3	Experimental Studies and Practical Applications.....	134
5.4.3.1	Cantilever Beams in Two Apartment Blocks, <i>Tilburg</i>	136
5.4.3.2	Gallery Slabs and Frames, <i>Groningen</i>	138
5.4.3.3	Abutments of a Post-Tensioned Bridge, <i>River Dommel</i>	139
5.4.3.4	Experimental Study.....	141
5.4.4	Selection Guidelines for Using Cathodic Protection Systems.....	147
5.4.5	Comparison between Different Corrosion Elimination Techniques.....	148
CHAPTER 6 MATERIALS AND TEST METHODS.....		150
6.1	Experimental Program.....	150
6.2	Concrete Mix Parameters.....	151
6.3	Reinforcing Steel.....	158
6.4	Properties of the Concrete Mixtures.....	161
6.4.1	Concrete Mix Design.....	162
6.4.1.1	Mix No. (1).....	162
6.4.1.2	Mix No. (2).....	163
6.4.1.3	Mix No. (3).....	163
6.4.1.4	Mix No. (4).....	164
6.5	Specimens Preparation.....	169
6.6	Accelerated Corrosion.....	171
6.6.1	Test Set-Up.....	172
6.7	Pull-Out Test.....	174
6.8	Percentage of Mass Loss.....	175
6.9	Bar Profile Loss.....	175
CHAPTER 7 TEST RESULTS AND DISCUSSION FOR ACCELERATED CORROSION SPECIMENS.....		176
7.1	Introduction.....	176
7.2	Current Measurement Results.....	176
7.2.1	Effect of Steel Types on the Current Measurements.....	177
7.2.2	Effect of Concrete Types on the Current Measurements.....	181
7.3	Pull-Out Test Results.....	185
7.3.1	Zero Corrosion Stage.....	186

7.3.2	Pre-cracking, Cracking and Severe Corrosion Stages.....	191
7.4	Effect of Corrosion on Concrete Reinforcement Mechanical Properties....	202
7.5	Effect of Corrosion on Concrete Reinforcement Physical Properties.....	209
CHAPTER 8 A NUMERICAL MODEL FOR STEEL-CONCRETE BOND.....		213
8.1	Background.....	213
8.2	Objective.....	213
8.3	Literature Review.....	214
8.4	Existing FE Models for Reinforced Concrete.....	217
8.5	Finite Element Modeling of Bond.....	219
8.6	Proposed Model.....	221
8.7	Corrosion Effect Model.....	221
8.7.1	Model (1): Elastic behavior for steel and concrete.....	223
8.7.1.1	Model description.....	223
8.7.1.2	Model Analysis.....	223
8.7.2	Model (2): Steel (elasto-plastic) and concrete (elastic).....	227
8.7.2.1	Model description.....	227
8.7.2.2	Model Analysis.....	227
8.7.3	Model (3): Steel (elastic) and concrete (elasto-plastic).....	231
8.7.3.1	Model description.....	231
8.7.3.2	Model Analysis.....	231
8.7.4	Model (4): Steel (elasto-plastic) and concrete (elasto-plastic).....	235
8.7.4.1	Model description.....	235
8.7.4.2	Model Analysis.....	236
8.7.5	Model (5): Steel (elasto-plastic) and concrete (elasto-plastic) 2D circular.....	239
8.7.5.1	Model description.....	239
8.7.5.2	Model Analysis.....	241
8.7.6	Model (6): Steel (elasto-plastic) and concrete (elasto-plastic) 2D quarter circle with increased mesh distribution.....	244
8.7.6.1	Model description.....	244
8.7.6.2	Model Analysis.....	244
8.7.7	Parametric study.....	246
8.7.7.1	Effect of concrete compressive strength.....	246
8.7.7.2	Comparison between experimental and finite element results....	248
8.8	Concrete Re-bar Bond Model.....	249
8.8.1	Parametric study.....	253
CHAPTER 9 CONCLUSIONS AND RECOMMENDATIONS.....		259
9.1	Summary.....	259
9.2	Conclusions.....	259
9.3	Recommendations for Future Work.....	268
REFERENCES.....		269
APPENDIX (A).....		277

LIST OF TABLES

Table 1.1: Buildings collapses in Egypt.....	3
Table 1.2: Monthly climatic data for Alexandria, Egypt.....	6
Table 3.1 Critical chloride content required to initiate the corrosion of the reinforcing steel.....	43
Table 3.2: Types of corrosion.....	46
Table 3.3: Chloride transport mechanisms.....	59
Table 3.4: Corrosion condition related to Open circuit potential (OPC) values.....	71
Table 3.5: Corrosion risk related to concrete resistivity.....	72
Table 3.6: Corrosion current vs. condition of the rebar.....	73
Table 3.7: Longitudinal pulse velocity vs. quality of concrete.....	76
Table 4.1: Properties of hardened concrete.....	89
Table 4.2: Test results from cylinder compression tests.....	93
Table 4.3: The pull-out test data for each concrete pour.....	94
Table 4.4: Strengths for No. 13 bars with 171 mm bonded length.....	99
Table 4.5: Strengths for No. 13 bars with 102 mm bonded length.....	99
Table 4.6: Strengths for No. 19 bars with 254 mm bonded length.....	100
Table 4.7: Strengths for No. 25 bars with 330 mm bonded length.....	101
Table 4.8: Strengths for No. 35 bars with 254 mm bonded length.....	102
Table 5.1: Variation of rate of rusting with time.....	112
Table 5.2: Spray-coating materials.....	116
Table 5.3: Calcium nitrite dosage rates.....	129
Table 5.4: Corrosion elimination techniques comparison.....	149
Table 6.1: Different types of concrete mixes used in the experimental program.....	151
Table 6.2: Different types of steel bars used in the experimental program.....	151

Table 6.3: Sieve analysis test results for sand sample (A).....	152
Table 6.4: Sieve analysis test results for sand sample (B).....	153
Table 6.5: Sieve analysis results for coarse aggregate sample.....	154
Table 6.6: Coarse aggregates test results.....	155
Table 6.7: Passing percentages of aggregate mix.....	155
Table 6.8: ESS for concrete aggregates.....	156
Table 6.9: Al-Arish ordinary Portland cement standard specifications.....	157
Table 6.10: Ordinary Portland cement standard specifications.....	157
Table 6.11: Characteristics of super plasticizer.....	158
Table 6.12: Mechanical properties of steel bars.....	159
Table 6.13: Results of slump tests for the fresh concrete.....	161
Table 6.14: Concrete mix proportions per cubic meter.....	165
Table 6.15: The results of compressive strength and splitting tensile strength tests for mix No. (1).....	167
Table 6.16: The results of compressive strength and splitting tensile strength tests for mix No. (2).....	167
Table 6.17: The results of compressive strength and splitting tensile strength tests for mix No. (3).....	168
Table 6.18: The results of compressive strength and splitting tensile strength tests for mix No. (4).....	168
Table 7.1: Distribution of circuits inside the corrosion tank.....	177
Table 7.2: Bond strength and shape of failure for each type of concrete and steel, zero corrosion.....	189
Table 7.3: Timing of corrosion stages for each type of concrete and steel bars.....	192
Table 7.4: Bond strength at several degrees of corrosion.....	200
Table 7.5: Bond strength as a percentage of zero corrosion values for different degrees of corrosion.....	201
Table 7.6: Mass loss of steel bars at different degrees of corrosion.....	211
Table 7.7: Rib profile loss of steel bars at different degrees of corrosion.....	212

Table 8.1: Values of parameters for CEB-FIP MC90 model.....	216
Table 8.2: Values of parameters in Engstrom’s Model.....	216
Table 8.3: Model No. (1) parameters.....	223
Table 8.4: Model No. (2) parameters.....	227
Table 8.5: Model No. (3) parameters.....	231
Table 8.6: Model No. (4) parameters.....	235
Table 8.7: Trials made to increase the finite model accuracy.....	255
Table 8.8: Calculated values of modulus of elasticity according to the ACI 318....	258

LIST OF FIGURES

Figure 1.1: Close up view of collapsed beams, Berlin Congress Hall.....	2
Figure 1.2: Collapse of four apartment buildings in Alexandria, July 2012.....	3
Figure 1.3: Rubble of eight story building collapse in Alexandria, January 2013.....	3
Figure 1.4: The location of Alexandria & Damietta on the Egyptian map.....	4
Figure 1.5: Concrete cover spalling, Alexandria.....	5
Figure 1.6: Deterioration of building's frontage, Alexandria.....	5
Figure 1.7: Total concrete cover spalling and exposure of the reinforcement to direct corrosion, Alexandria.....	7
Figure 2.1: Bond force transfer mechanism.....	12
Figure 2.2a: Average load-loaded end slip curves for No. 8 ASTM A615 reinforcing bars in a beam-end specimen.....	13
Figure 2.2b: Average load-unloaded end slip curves for No. 8 ASTM A615 reinforcing bars in a beam-end specimen.....	14
Figure 2.3: Bond stress-slip curve for bar loaded monotonically and failing by pull-out.....	15
Figure 2.4: Variation in bond stress with rib face angle.....	17
Figure 2.5: Definition of R_r	18
Figure 2.6: Effect of rib face angle.....	19
Figure 2.7: Effect of rib spacing.....	20
Figure 2.8: Effect of rib height.....	20
Figure 2.9: Deformation patterns of bars for pull-out test.....	22
Figure 2.10: Relationship between BA^* and bond stress.....	22
Figure 2.11: Details of specimens.....	23
Figure 2.12: Effect of concrete strength on bond strength at splitting.....	24
Figure 2.13: Relationship between maximum shear strength and concrete strength.....	24
Figure 2.14: The influence of casting position on bond performance.....	24

Figure 2.15: Bond-slip relationship for 16 mm plain rounded bars in different casting positions.....	25
Figure 2.16: Bond-slip relationship for plain rounded bars as affected by settlement of fresh concrete.....	26
Figure 2.17: Variation of steel and bond forces in reinforced concrete member subjected to pure bending.....	28
Figure 2.18: Local bond stress-slip law.....	30
Figure 2.19a: Bar-concrete slipping and wedging action of the bar.....	31
Figure 2.19b: Friction and bearing action.....	31
Figure 2.19c: Transverse cracking and splitting.....	31
Figure 2.20: Load-slip curve for cyclic loading with different rib angles.....	32
Figure 2.21: Modes of bond failure.....	33
Figure 2.22: Cracking and damage mechanisms in bond.....	34
Figure 3.1: Film thickness-potential and current density.....	36
Figure 3.2: Iron oxide film around the steel bar.....	37
Figure 3.3: Histogram of the free chloride threshold from the values published.....	44
Figure 3.4: Histogram of the total chloride threshold from the values published.....	44
Figure 3.5: Anodes and cathodes in corrosion processes.....	45
Figure 3.6: Simple deterioration model.....	48
Figure 3.7: Dimensional range of solids and pores in hydrated cement paste.....	50
Figure 3.8: Schematic representation of the volumetric proportions in cement paste before and during hydration.....	52
Figure 3.9: Example of micro-structure of hydrated cement paste.....	52
Figure 3.10: Influence of the water/cement ratio and curing on the distribution of pore size in hydrated cement pastes.....	54
Figure 3.11: Principle factors involved in the transport processes in concrete.....	55
Figure 3.12a: Influence of capillary porosity on strength and permeability of cement paste.....	56
Figure 3.12b: Capillary porosity derived from a combination of water/cement ratio and degree of hydration.....	56

Figure 3.13: Marine exposure zones of concrete structures.....	57
Figure 3.14: Concrete cover spalling.....	58
Figure 3.15: Abrasion and cement decomposition in tidal zone.....	58
Figure 3.16: Electrochemical reactions at the embedded steel bar surface.....	60
Figure 3.17: Variation of porosity with depth of concrete slabs cured using different methods.....	61
Figure 3.18: Current readings for NPC concrete (w/c=0.52) specimens with different steel types for pre-cracking stage.....	63
Figure 3.19: Current readings for NPC concrete (w/c=0.52) specimens with different steel types for cracking stage.....	63
Figure 3.20: Current readings for NPC concrete (w/c=0.52) specimens with different steel types for severe corrosion stage.....	64
Figure 3.21: Current readings for NPC concrete (w/c=0.32) specimens with different steel types for pre-cracking stage.....	64
Figure 3.22: Current readings for NPC concrete (w/c=0.32) specimens with different steel types for cracking stage.....	65
Figure 3.23: Current readings for NPC concrete (w/c=0.32) specimens with different steel types for severe corrosion stage.....	65
Figure 3.24: Current readings for S.F concrete specimens with different steel types for pre-cracking stage.....	66
Figure 3.25: Current readings for S.F concrete specimens with different steel types for cracking stage.....	66
Figure 3.26: Current readings for S.F concrete specimens with different steel types for severe corrosion stage.....	67
Figure 3.27: Current readings for F.A concrete specimens with different steel types for pre-cracking stage.....	67
Figure 3.28: Current readings for F.A concrete specimens with different steel types for cracking stage.....	68
Figure 3.29: Current readings for F.A concrete specimens with different steel types for severe corrosion stage.....	68
Figure 3.30: Schematic representation of (OCP) measurements.....	70
Figure 3.31: Schematic representation of (SP) measurements.....	71

Figure 3.32: Circuit for electrical resistance measurements.....	72
Figure 3.33: Linear polarization resistance (LRP) measurement.....	73
Figure 3.34: ECI sensor during operation.....	74
Figure 3.35: Cover meter.....	75
Figure 4.1: Supplementary cementing materials.....	78
Figure 4.2: Change in pore size distribution of cement paste with varying pozzolan.....	80
Figure 4.3: Effect of silica fume on the electrical resistance of concrete.....	82
Figure 4.4a: Gaining of strength for fly ash concrete mixture using 50% fly ash and w/cm=0.45.....	83
Figure 4.4b: Gaining of strength for fly ash concrete mixture using 45% fly ash and w/cm=0.40.....	84
Figure 4.4c: Gaining of strength for fly ash concrete mixture using 50% fly ash and w/cm=0.34.....	84
Figure 4.5: Effect of fly ash on ASR expansion.....	84
Figure 4.6: Effect of low-calcium fly ash on sulfate resistance.....	85
Figure 4.7: Typical pull-out specimen.....	86
Figure 4.8: Beam anchorage specimen.....	87
Figure 4.9: Beam end test.....	87
Figure 4.10: Splice specimen.....	88
Figure 4.11: Variation of bond stress with slip for 0.52 normal concrete mix with different steel types.....	90
Figure 4.12: Variation of bond stress with slip for 0.32 normal concrete mix with different steel types.....	90
Figure 4.13: Variation of bond stress with slip for silica fume concrete mix with different steel types.....	90
Figure 4.14: Variation of bond stress with slip for fly ash concrete mix with different steel types.....	91
Figure 4.15: Compressive strength vs. test day plot for all cylinders mixes.....	93
Figure 4.16: Typical load vs. slip plot.....	94

Figure 4.17: Bond strength components.....	95
Figure 4.18: Beam end test specimens.....	97
Figure 4.19: No. 35 test bar photographs.....	97
Figure 4.20: Test setup.....	98
Figure 4.21: Measured relations between applied tension force and slip at the loaded end of No. 25 test bars.....	103
Figure 4.22: Test setup.....	103
Figure 4.23: Reinforcing bars deformation patterns.....	104
Figure 4.24: Typical plot of load-slip relationships for different coating thicknesses.....	104
Figure 4.25: Relationship between the ultimate bond strength and degrees of corrosion.....	106
Figure 4.26: Relationship between load and slip for 0 to 6 % (percentage of weight loss).....	106
Figure 4.27: Relationship between load and slip at percentage of weight loss higher than 6%.....	107
Figure 4.28: Effect of rib profile loss on ultimate bond strength.....	107
Figure 4.29: Influence of corrosion mass loss on bond strength.....	108
Figure 4.30: Effect of corrosion on load-slip behavior.....	108
Figure 4.31: Variation of bond stress with slip for different steel types.....	109
Figure 4.32: Relationship between bond stress and different degrees of corrosion.....	109
Figure 5.1: The evolution of a porous anodic film on aluminum as a function of the sealing time at 85° C.....	117
Figure 5.2: Current flow and distribution in cathodic protection of a pipeline.....	130
Figure 5.3: Evans diagram illustrating the increasing CP current requirements as the potential of the structure is lowered to reduce the anodic dissolution rate.....	131
Figure 5.4: Cathodic protection diagram illustrating the current flow from an external supplement anode to the embedded reinforcement in the structure resulting in cathodic protection.....	132

Figure 5.5: Transfer of electrons between concrete reinforcement and the new added anode.....	133
Figure 5.6: The case of existing deteriorated conditions.....	135
Figure 5.7: The case of corrosion prevention.....	135
Figure 5.8: Cantilever beam with strip anode in cement-filled borehole.....	137
Figure 5.9: Average and standard derivation of depolarization of 34 zones.....	137
Figure 5.10: Layout of slabs and frames with conductive coating on all faces except top face of slabs.....	139
Figure 5.11: Cross section in bridge abutment.....	140
Figure 5.12: Rebar skeleton arrangement before placing concrete.....	142
Figure 5.13: Slab with chloride and without cathodic protection.....	142
Figure 5.14: Slab with chloride and zinc overlay with cathodic protection.....	143
Figure 5.15: Slab with chloride and conductive polymer overlay with cathodic protection.....	143
Figure 5.16: Effect of time on resistivity and potential of embedded steel in chloride free concrete.....	144
Figure 5.17: Effect of time on resistivity and potential of embedded steel in chloride contaminated concrete.....	145
Figure 5.18: Effect of time on resistivity and potential of embedded steel in chloride contaminated concrete with CP for various distances from the anode.....	145
Figure 5.19: Effect of cathodic protection on the potential of steel in slab coated with mortar containing zinc in chloride contaminated concrete.....	146
Figure 5.20: Effect of cathodic protection on the potential of steel in slab with conductive paint in the middle of the cover in chloride contaminated concrete.....	146
Figure 5.21: Effect of time on the current flowing in slabs with cathodic protection.....	147
Figure 6.1: Grading curve for sand sample (A).....	152
Figure 6.2: Grading curve for sand sample (B).....	153
Figure 6.3: Grading curve for coarse aggregate sample.....	154
Figure 6.4: Aggregates grading curve.....	156

Figure 6.5: Al-Arish Portland cement.....	157
Figure 6.6: Different types of steel bars.....	158
Figure 6.7: Stress-strain curve for PL-UC.....	159
Figure 6.8: Stress-strain curve for DF-UC.....	160
Figure 6.9: Stress-strain curve for DF-C.....	160
Figure 6.10: Electrical mixer.....	161
Figure 6.11: Tensile splitting test.....	166
Figure 6.12: Cylindrical concrete specimens.....	169
Figure 6.13: Interface between the protruding steel bar and the surface of the concrete.....	170
Figure 6.14: A circular steel piece to maintain bar verticality.....	170
Figure 6.15: Curing of concrete specimens.....	171
Figure 6.16: Accelerated corrosion tank components.....	172
Figure 6.17: 12V power supply.....	173
Figure 6.18: Digital multi-meter.....	173
Figure 6.19: Accelerated corrosion tank set-up.....	173
Figure 6.20: Instron Universal testing machine.....	174
Figure 7.1: Accelerated corrosion tank circuits division.....	176
Figure 7.2: Current readings vs. immersion time for 30 MPa concrete mixes (w/c=0.32) with different types of steel bars.....	178
Figure 7.3: Current readings vs. immersion time for 44 MPa concrete mixes (w/c=0.52) with different types of steel bars.....	178
Figure 7.4: Current readings vs. immersion time for 44 MPa concrete mixes (w/c=0.32) with different types of steel bars.....	179
Figure 7.5: Current readings vs. immersion time for 60 MPa concrete mixes (w/c=0.32) with different types of steel bars.....	179
Figure 7.6: Cracks passing through the un-coated end of epoxy coated bars.....	180
Figure 7.7: Current readings vs. immersion time for un-coated plain bars with different types of concrete mixes.....	182

Figure 7.8: Current readings vs. immersion time for un-coated deformed bars with different types of concrete mixes.....	182
Figure 7.9: Current readings vs. immersion time for epoxy coated deformed bars with different types of concrete mixes.....	183
Figure 7.10: Sudden cracks for mix No. (4) un-coated samples in the accelerated corrosion tank.....	184
Figure 7.11: A pull-out specimen loaded in the Universal testing machine.....	185
Figure 7.12: Load-slip relationship for 30MPa, 0.32 w/c mix with different types of steel bars, <i>Zero corrosion stage</i>	187
Figure 7.13: Load-slip relationship for 44MPa, 0.52 w/c mix with different types of steel bars, <i>Zero corrosion stage</i>	187
Figure 7.14: Load-slip relationship for 44MPa, 0.32 w/c mix with different types of steel bars, <i>Zero corrosion stage</i>	188
Figure 7.15: Load-slip relationship for 60MPa, 0.32 w/c mix with different types of steel bars, <i>Zero corrosion stage</i>	188
Figure 7.16: Small cracking.....	190
Figure 7.17: Longitudinal cracking.....	190
Figure 7.18: Total splitting.....	190
Figure 7.19: Sudden crushing.....	190
Figure 7.20: Pre-cracking stage.....	191
Figure 7.21: Cracking stage.....	191
Figure 7.22: Severe corrosion stage.....	192
Figure 7.23: Corrosion durations for un-coated plain bars embedded in different concrete strength mixes with the same water/cement ratio 0.32.....	193
Figure 7.24: Corrosion durations for un-coated deformed bars embedded in different concrete strength mixes with the same water/cement ratio 0.32.....	193
Figure 7.25: Corrosion durations for epoxy coated deformed bars embedded in different concrete strength mixes with the same water/cement ratio 0.32.....	193
Figure 7.26: Corrosion durations for un-coated plain bars embedded in different water/cement ratios concrete mixes with the same strength (44MPa).....	194
Figure 7.27: Corrosion durations for un-coated deformed bars embedded in different water/cement ratios concrete mixes with the same strength (44MPa).....	194

Figure 7.28: Corrosion durations for epoxy coated deformed bars embedded in different water/cement ratios concrete mixes with the same strength (44MPa).....	194
Figure 7.29: Bond-slip relationship for Mix. No. (1) Un-coated plain bars.....	195
Figure 7.30: Bond-slip relationship for Mix. No. (1) Un-coated deformed bars.....	195
Figure 7.31: Bond-slip relationship for Mix. No. (1) Epoxy coated deformed bars.....	196
Figure 7.32: Bond-slip relationship for Mix. No. (2) Un-coated plain bars.....	196
Figure 7.33: Bond-slip relationship for Mix. No. (2) Un-coated deformed bars.....	196
Figure 7.34: Bond-slip relationship for Mix. No. (2) Epoxy coated deformed bars.....	197
Figure 7.35: Bond-slip relationship for Mix. No. (3) Un-coated plain bars.....	197
Figure 7.36: Bond-slip relationship for Mix. No. (3) Un-coated deformed bars.....	197
Figure 7.37: Bond-slip relationship for Mix. No. (3) Epoxy coated deformed bars.....	198
Figure 7.38: Bond-slip relationship for Mix. No. (4) Un-coated plain bars.....	198
Figure 7.39: Bond-slip relationship for Mix. No. (4) Un-coated deformed bars.....	198
Figure 7.40: Bond-slip relationship for Mix. No. (4) Epoxy coated deformed bars.....	199
Figure 7.41: Un-coated bars, pre-cracking stage.....	202
Figure 7.42: Uniformly corroded sample, plain bars, cracking stage.....	202
Figure 7.43: Uniformly corroded sample, un-coated bars, cracking stage.....	203
Figure 7.44: Concentrated corrosion, epoxy coated bars, cracking stage.....	203
Figure 7.45: Un-coated bars, severe corrosion stage.....	203
Figure 7.46: Un-coated plain bars, severe corrosion stage.....	204
Figure 7.47: Total corrosion at bar end, epoxy coated bars, severe corrosion stage.....	204
Figure 7.48: Stress-strain curve for plain bars at each degree of corrosion, Mix. No. (1).....	205
Figure 7.49: Stress-strain curve for un-coated deformed bars at each degree of corrosion, Mix. No. (1).....	205

Figure 7.50: Stress-strain curve for epoxy coated deformed bars at each degree of corrosion, Mix. No. (1).....	205
Figure 7.51: Stress-strain curve for plain bars at each degree of corrosion, Mix. No. (2).....	206
Figure 7.52: Stress-strain curve for un-coated deformed bars at each degree of corrosion, Mix. No. (2).....	206
Figure 7.53: Stress-strain curve for epoxy coated deformed bars at each degree of corrosion, Mix. No. (2).....	206
Figure 7.54: Stress-strain curve for plain bars at each degree of corrosion, Mix. No. (3).....	207
Figure 7.55: Stress-strain curve for un-coated deformed bars at each degree of corrosion, Mix. No. (3).....	207
Figure 7.56: Stress-strain curve for epoxy coated deformed bars at each degree of corrosion, Mix. No. (3).....	207
Figure 7.57: Stress-strain curve for plain bars at each degree of corrosion, Mix. No. (4).....	208
Figure 7.58: Stress-strain curve for un-coated deformed bars at each degree of corrosion, Mix. No. (4).....	208
Figure 7.59: Stress-strain curve for epoxy coated deformed bars at each degree of corrosion, Mix. No. (4).....	208
Figure 7.60: A friable layer formed around the bar at further degrees of corrosion.....	210
Figure 8.1: Bilinear bond slip relationships for three, five and six segments.....	215
Figure 8.2: CEB-FIP MC90 model.....	215
Figure 8.3: Engstrom's model.....	216
Figure 8.4: FE model according to Bresler & Bertero.....	220
Figure 8.5: FE model according to Nilson.....	220
Figure 8.6: The modified double spring element using possible unidirectional spring element configuration.....	220
Figure 8.7: 2D plan of the concrete cylinder and the embedded bar.....	222
Figure 8.8: 2D model geometry and Abaqus mesh.....	222
Figure 8.9: Model No. (1) analysis.....	224

Figure 8.10: Node behaviour for Model No. (1).....	225
Figure 8.11: Stress-strain relationship for 240/350 steel bar.....	228
Figure 8.12: Model No. (2) analysis.....	228
Figure 8.13: Node behaviour for Model No. (2).....	229
Figure 8.14: Stress-strain relationship for concrete.....	232
Figure 8.15: Model No. (3) analysis.....	232
Figure 8.16: Node behaviour for Model No. (3).....	233
Figure 8.17: Model No. (4) analysis.....	236
Figure 8.18: Element behaviour for Model No. (4).....	237
Figure 8.19: Model No. (5) analysis.....	238
Figure 8.20: The 2D model of cross-section (Model No. 5).....	239
Figure 8.21: Concrete axial strain in x-direction.....	240
Figure 8.22: Elements behaviour for Model No. (5).....	242
Figure 8.23: Model No. (6) Abaqus mesh.....	244
Figure 8.24: Concrete axial strain in x-direction, Model No. (6).....	245
Figure 8.25: Tensile stresses at an interface element for different concrete strengths.....	247
Figure 8.26: Axial strain at an interface element for different concrete strengths....	247
Figure 8.27: Crack initiation behaviour in the experimental and finite element models.....	248
Figure 8.28: ABAQUS model for the concrete re-bar bond simulation.....	249
Figure 8.29: Different parts of the pull-out model (16mm steel bar, interface elements, and 100mm concrete cylinders).....	250
Figure 8.30: Stresses acting on the steel bar, S_{misses}	251
Figure 8.31: Stresses acting on the concrete cylinder.....	252
Figure 8.32: Shear stresses at the interface element	253
Figure 8.33: Load-slip relationship for different strength concrete samples.....	254
Figure 8.34: Comparison between experimental and finite results.....	254

Figure 8.35: Finite element model iterations for 30MPa.....	256
Figure 8.36: Finite element model iterations for 44MPa.....	256
Figure 8.37: Finite element model iterations for 60MPa.....	256
Figure 8.38: Concrete compressive strength vs. Interface elements stiffness.....	257



INTRODUCTION

1.1 General

Recently the aspects of concrete durability and performance have become a major subject of discussion especially when the concrete is subjected to a severe environment. Corrosion of steel bars is the main factor influencing both the concrete durability and strength. The corrosion products of the steel reinforcement can expand four to five times its original volume, developing high pressures within the concrete, which cause cracking and spalling of the concrete cover and expose the rebar to further corrosion activity.

The potential consequences of the corrosion problem can be summed up in the continuous reduction in strength, stiffness, durability and designed life time of concrete structural elements reinforced with conventional steel. Corrosion of reinforcing steel bars in concrete has caused catastrophic failures in some specific cases, resulting in injury and death, such as the collapse of the Berlin Congress Hall as shown in Fig. 1.1 *Isecke (1982)* and of a parking in Minnesota, *Borgard et al. (1990)*.

The down fall of the Berlin Congress Hall was due to poor structural design that failed to address corrosion prevention. Each combining element called for protection that would provide sufficient coverage against corrosive events. Such however was not the case. The vertical movements of the arches created shear forces that placed stress on the tendons causing cracks in the slabs. Such stresses were amplified by the absence of sufficient protection against moisture and other precipitation agents such as: temperature changes, stresses, wind, snow, vibrations, and settlements, which caused the thin shell roof to crack. Over time these elements were able to affect the tensioning steel, leading to severe corrosion that ultimately led to its collapse.

One of the most evident modern corrosion disasters is the present state of degradation of the North American infrastructure. The structural integrity of thousands of bridges, roadbeds, overpasses and other concrete structures has been



impaired by corrosion, urgently requiring expensive repairs to ensure public safety. But the problems of corroding reinforced concrete extend much beyond the transportation infrastructure. A survey of collapsed buildings during the 1974 to 1978 period in England showed that the immediate cause of failure of at least eight structures, which were 12 to 40 years old, was corrosion of reinforcing or pre-stressing steel, *Roberge (1999)*.



Fig. 1.1: Close up view of collapsed beams, Berlin Congress Hall

Deterioration of parking garages has become a major concern in Canada. Of the 215 garages surveyed recently, almost all suffered varying degrees of deterioration due to reinforcement corrosion, which was a result of design and construction practices that fell short of those required by the environment. It is also stated that almost all garages in Canada built until very recently by conventional methods will require rehabilitation at a cost to exceed \$3 billion, *Roberge (1999)*.

According to the Federal Highway Association, the infrastructure deficiencies due to corrosion in the United States present a \$300 billion per year at 1995 prices *Roberge (1999)* and \$1.3 trillion according to *Elsener (2001)*. In Canada, however, there is no accurate number of the infrastructure deficiency, but some studies found that the cost of rehabilitation for corrosion of reinforcing steel is estimated to be about \$3.0 billion per year in Canada, *Davis (2000)*.

In Egypt the disaster exceeds the value of money and extends to human lives. In the last decade many reinforced concrete buildings collapsed with a majority located in seafront zones (Figs 1.2 and 1.3). Over eighty percent of these collapses were at



Alexandria and Damietta as shown in Table 1.1. This high percentage highlights the importance of studying the common factors that lead to the collapse of those buildings.



Fig. 1.2: Collapse of four apartment buildings in Alexandria, July, 2012 (*El-Masry El-Youm*)



Fig. 1.3: Rubble of eight story building collapse in Alexandria, Egypt, Jan. 16, 2013 (*El-Masry El-Youm*)

Table 1.1: Buildings collapses in Egypt.

Date	Description
March 2002	Two buildings collapsed within 24 hours in the industrial city of Damietta, killing a total of 27 people and 25 people were seriously injured.
December 2007	Twenty five years old 12 story building collapsed in Alexandria with 23 people killed
October 2008	Twelve people were killed and six were injured after an old apartment building collapsed in Alexandria.
December 2010	Seven people killed and ten wounded in a factory building collapse in Alexandria
December 2011	Three story residential building collapsed in Alexandria. One person was killed and three were severely wounded.
January 2012	Collapse of a building in the center of Damietta with six killed and twenty eight injured.
July 2012	Nine people killed and ten wounded in collapse of four buildings in Alexandria.
September 2012	Five story building collapsed with at least five people injured.
September 2012	Four story building collapsed in downtown Assiut with nine people killed.
October 2012	Collapse of three story building located on Mahmoudeya water channel, Alexandria.
January 2013	Collapse of five years old, eight story building in Mamora, Alexandria. Twenty eight dead and twelve injured.
February 2013	One killed and five injured in a building collapse in Moharam Bek, Alexandria.

Alexandria and Damietta are both considered as coastal cities located on the Mediterranean Sea as shown in Fig. 1.4. The climate in these two cities has the characteristics of mild weather, with variable rainy winters and hot summers that at times, can be very humid. Alexandria experiences violent storms, rain and sometimes



hail during the cooler months. The average annual rainfall is around 200 millimeters but can be as high as 417 millimeters. Table 1.2 shows the monthly climatic data for Alexandria as reported by the World Meteorological Organization (*Hong Kong Observatory 1961-1990*).



Fig. 1.4: The location of Alexandria and Damietta on the Egyptian map

Marine atmosphere is laden with fine particles of sea mist carried by the wind to settle on exposed surfaces as salt crystals. The quantity of salt deposited can vary greatly with wind velocity and it may, in extreme weather conditions, even form a very corrosive salt crust. The quantity of salt contamination decreases with distance from the ocean, and is greatly affected by wind currents. The marine atmosphere also includes seafront zones where splashing and heavy sea sprays are encountered. Buildings located in these splash zones are indeed subjected to the worst conditions of intermittent immersion with wet and dry cycling of the corrosive agent. Coastal regions like Alexandria and Damietta are salt-laden environments with high relative humidity that reaches 73% in some months of the year. The environmental impacts in these regions are extremely high compared to other places in Egypt (Figs. 1.5 and 1.6). Usually under such conditions, a special design for concrete mix and good quality control during the building construction would control the effect of those environmental impacts.



A study was made by *Salah abd el Haleem* concerning the collapse of buildings in Egypt, especially those in Alexandria. This study stated that there were two main factors that must be studied. One of these was the type of steel reinforcement used, and the other was the type of cement and its quantity in the concrete mix. In Egypt the reinforcement bars used are carbon steel with high percentage of carbon. The standard percentage of carbon ranges from 3 to 4%, and according to this study, the rate of corrosion is directly proportional to the percentage of carbon used.



Fig. 1.5: Concrete cover spalling, Alexandria, Egypt



Fig. 1.6: Deterioration of building's frontage, Alexandria, Egypt

It should be emphasized that the reinforcing steel is provided in reinforced concrete to resist the tensile forces, and to produce controlled cracking within that zone. However, corrosion not only deteriorates the steel bar and its function of transferring the tensile stresses, but it also deteriorates the concrete by spalling of the cover (Fig. 1.7). Therefore, corrosion of the reinforcement has a strong influence on the bond behavior at the interface between the steel reinforcement and concrete.

Bond stress is the shear stress over the surface of the bar, and is defined as the change in the force within the reinforcing bar divided by the area of that bar surface over which the change in the force takes place, *Aal Hassan (2003)*. Bond stress initially comes from weak chemical bonds between steel and hardened hydrated cement paste in the concrete, but this resistance is broken at a very low stress. Once slip occurs, friction contributes to the bond, but with increasing slip between bar and concrete, bond comes to depend principally on the bearing of the lugs on the concrete, or mechanical interlock of the ribs rolled on the surface of the bar with the concrete. In this stage, the reinforcing bar generates bursting forces tends to split the



surrounding concrete. However the resistance provided by the concrete cover and the confining reinforcement may limit the failure load.

Table 1.2: Monthly climatic data for Alexandria, Egypt

Month	Jan	Feb	Mar	Apr	May	Jun	Jul	Aug	Sep	Oct	Nov	Dec	Year
Record high °C	29	33	40	41	45	44	43	39	41	38	36	29	
Average high °C	18.4	19.3	20.9	24.0	26.5	28.6	29.7	30.4	29.6	27.6	24.1	20.1	24.9
Daily mean °C	13.4	13.9	15.7	18.5	21.2	24.3	25.9	26.3	25.1	22.0	18.7	14.9	20.0
Average low °C	9.1	9.3	10.8	13.4	16.6	20.3	22.8	23.1	21.3	17.8	14.3	10.6	15.8
Record low °C			2	4	7	12	17	18	14	11	1	1	
Rainfall mm	52.8	29.2	14.3	3.6	1.3	0.01	0.03	0.1	0.8	9.4	31.7	52.7	195.9
Avg. rainy days (≥ 0.01 mm)	11.0	8.9	6.0	1.9	1.0	0.04	0.04	0.04	0.2	2.9	5.4	9.5	46.92
Mean monthly sunshine hours	192	217	248.0	273	316.2	354	362.7	344	297	282	225	195	3,307
Relative Humidity (%)	70	68	66	66	68	71	73	72	68	68	69	72	69.3

According to the ASTM, corrosion is defined as “the chemical or electrochemical reaction between a material, usually a metal, and its environment that produces a deterioration of the material and its properties.” For steel embedded in concrete, corrosion results in the formation of rust which has two to four times the volume of the original steel and none of its good mechanical properties, *Perenchio (1994)*. Corrosion also produces pits or holes in the surface of reinforcing steel, reducing strength capacity as a result of the reduced cross-sectional area.

Corrosion could be expected to affect bond strength between the steel reinforcement and concrete. The expansion due to the corrosion products at first increases the radial stresses between the bars and concrete and hence increases the frictional component of bond. However, further corrosion develops longitudinal



cracking and reduction in the resistance to the bursting forces generated around the steel bar. A firmly adherent layer of rust may contribute to an enhancement in bond strength at early stages of corrosion, *Al- Sulaimani et al (1990)*, but at more advanced stages of corrosion, weak and friable material between bar and concrete will certainly be at least partially responsible for the reduction in bond strength, *Cabrera and Ghodussi (1992)*.



Fig. 1.7: Total concrete cover spalling and exposure of the reinforcement to direct corrosion, Alexandria, Egypt

Corrosion reduces the ribs height of the deformed bar which causes reduction in the contact area between the ribs and the concrete leading to reduction in the bond strength. Corrosion also may affect the rib face angle in the advanced stages; moreover ribs of deformed bars will eventually be lost at high level of corrosion. Corrosion of reinforced bars is usually associated with the increase of the crack width. The increase of the corrosion products around the bar leads to increase of bursting force and tension cracking of the surrounding concrete, as the corrosion increases, the cracks width becomes wider and the bond strength decreases.



Structural weakening caused by corrosion can reduce a structure's service life to only 15-25 years well below the design life that structures are typically designed for. Corrosion usually occurs when structures are located within the vicinity of coastal areas, brackish rivers or wherever there is exposure to a source of chloride. Patching of damaged areas or sealing them does not stop the corrosion process, and deterioration will continue to spread to other areas.

1.2 Scope and Objectives

The main objective of this research is to study the effect of corrosion on bond strength using four different types of concrete with three different types of steel embedded. The study is conducted for four levels of corrosion, from un-corroded bars to severely corroded bars.

A comprehensive experimental program will be implemented to test the effect of certain parameters as water/cement ratio, concrete strength, type of steel reinforcement and coating material. Using the data obtained from the experimental program, a finite element model will be developed to simulate the behavior of full scale buildings subjected to corrosion of steel reinforcement and its effect on the overall stability of the structure.

1.3 Thesis Structure

The thesis consists of nine chapters; a brief description of the contents of each chapter is included.

Chapter 1: Introduction

This chapter gives an introduction to the research and the problem statement including a case study of buildings in Egypt at sea side that were affected severely by the reinforcement corrosion.



Chapter 2: The bond mechanism

This chapter deals with the following; description of the bar-concrete interaction, the effect of bar profile, shape and geometry on the bond strength, and the effect of casting position on the bond strength.

Chapter 3: Mechanisms of steel corrosion

This chapter deals with the following; illustration of the steel corrosion formation, factors affecting the corrosion and obvious risks associated with steel corrosion in concrete.

Chapter 4: Bond performance in different concrete and steel types

This chapter deals with the following; the performance of bond in high performance concrete, the performance of bond for epoxy-coated bars and the performance of bond for corroded bars.

Chapter 5: Elimination of steel corrosion

This chapter deals with the following; description of the different types of corrosion inhibitors and illustrating how to choose the best technique for each type of structures.

Chapter 6: Materials and test methods

This chapter deals with the following; description of the research experimental work, the concrete mix parameters, the physical, chemical, and mechanical properties of the materials used, the properties of the concrete mixture including the test results of the fresh and hardened concrete, and description of specimens preparation and the tests setup.

Chapter 7: Test results and discussion for accelerated corrosion specimens

This chapter summarizes the test results of the following; the current measurements for the specimens tested and comparison of the corrosion times, the results of the pullout tests for un corroded bars and for different degrees of bars corrosion, a comparison between the reduction of tensile strengths for different



types of steel bars at different degrees of corrosion and a comparison between the bond strength of the plain and deformed steel bars, also between the coated and un coated steel bars at different degrees of corrosion as a percentage of the weight loss and the percentage of rib profile loss.

Chapter 8: A numerical model for steel-concrete bond

The primary objectives of this chapter are to develop a finite element model which could correctly simulate the bond-slip relationship in a reinforced concrete member, to accurately predict the level of stress transferred by the bond, and to show how to introduce the effect of steel reinforcement corrosion on the behavior of RC members. This model will be based on the results obtained from the physical model of the pull-out samples. Other objectives are comparing previous RC models that included bond behavior, and to select the best modeling techniques available to accurately reflect the bond behavior.

Chapter 9: Conclusions and recommendations

The conclusions that will be drawn from the investigation, and suitable recommendations for further research will be made in this chapter.



THE BOND MECHANISM

2.1 Introduction

Bond between reinforcement and concrete is necessary to ensure composite action of the two materials. The normal assumptions of plain section behavior used in section analysis and design rely on composite interaction being achieved. Bond stress is the shear stress over the surface of the bar, which is a considerably simplified representation of the actual conditions. Bond stress is defined as the change in the force within the reinforcing bar divided by the area of that bar surface over which the change in the force takes place. In other words, bond stress is the shear stress transferred from the concrete to the reinforcing bar to change the bar stress from point to point which depends on the development length and the change in the bending moment along the member.

Bond stress initially comes from the weak chemical bonds between the steel and the hardened hydrated cement paste of that concrete, but with a little increase of the applied load on the steel bar this resistance is lost. Once slip occurs, friction contributes to the bond, but with increasing slip between the bar and the concrete, bond resistance is derived principally from the bearing, or mechanical interlock, of the ribs on the surface of the bar with the concrete. At this stage, the reinforcing bar generates bursting forces results from the horizontal component of the force acting between the concrete and the rib face angle. This force tends to split the surrounding concrete, but the resistance provided by the concrete cover and the confining reinforcement to these bursting forces may limit the failure load.

2.2 Bond Between Reinforcing Steel and Concrete

Bond is the interaction between the reinforcing steel and the surrounding concrete where the forces are transferred from concrete to steel and vice versa, *Amleh and Gosh (2006)*. However, the slip is the relative movement of the bar that takes place with respect to the surrounding concrete when subjected to external forces.

The force in the steel bar that is transmitted to the surrounding concrete by bond can be classified into three components: (a) Chemical adhesion, (b) Friction, (c) Mechanical interlock between the concrete and the rebar (Fig. 2.1).

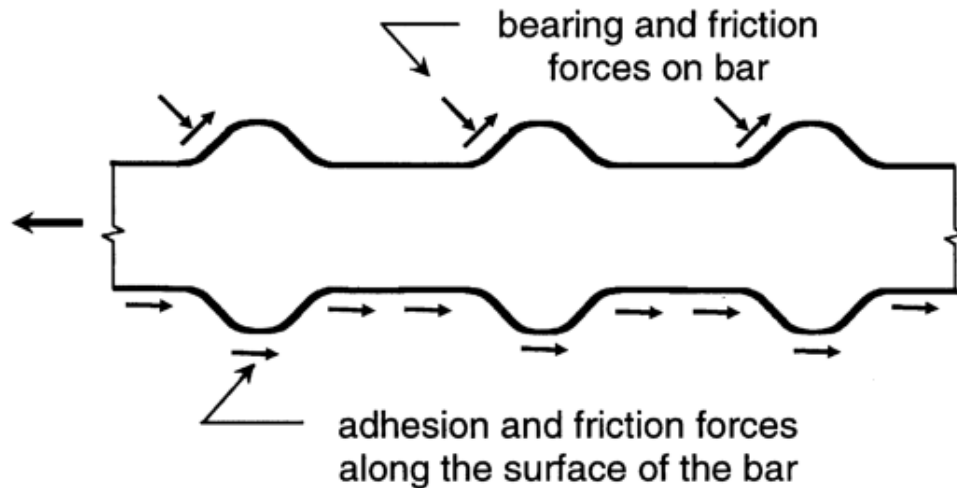


Fig. 2.1: Bond force transfer mechanism
[*Bond and Development of Straight Reinforcing Bars in Tension, ACI Committee 408*]

2.2.1 Chemical Adhesion

A relatively weak bond created on the interface between the steel bar and the surrounding concrete. This bond component can be easily lost due to the service load or shrinkage of concrete.

2.2.2 Friction

Unlike the adhesion bond, the friction bond depends mainly on the physical characteristics of the steel bar surface. This means that the component of friction bond increases as the roughness of the surface increases. This can happen in the stage of steel passivation where a thin passive film is formed at the interaction between the bar and the surrounding concrete before the corrosion is initiated.

2.2.3 Mechanical Interlock

This type of bond is due to the mechanical interlocking between the steel ribs and the concrete. The profile of the steel bar and the geometry of the ribs dictate the



amount of the mechanical bond generated between the steel bar and the concrete. At higher loading levels, the bearing against the ribs is considered the most significant stress transfer mechanism.

Bond of plain bars depends primarily on the first two components in addition to the effect of the end anchorage. Deformed bars, however, depend primarily on the mechanical interlocking in addition to chemical adhesion and friction as secondary ones.

Bond force-slip and bond stress-slip curves can be used to better understand the nature of bond response. In their simplest and most widely used form, the curves are based on known bar forces, such as obtained in the beam-end and beam anchorage specimens. Bar forces are compared with the external slip of the reinforcing bars, measured with respect to the concrete at either the loaded or unloaded end of the bar. Examples of bar force loaded end and unloaded end slip curves are shown in Figs. 2.2a and 2.2b, respectively. The loaded end bond force-slip curve shows a lower initial stiffness than the unloaded end curve. The difference represents the lengthening of the reinforcing bar between the two points of slip measurements.

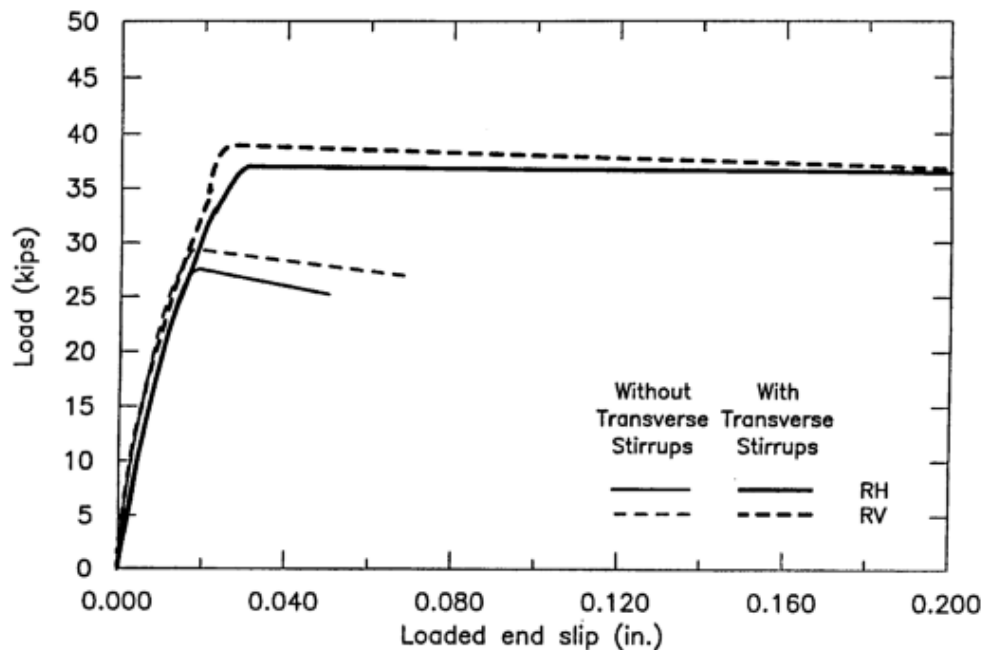


Fig. 2.2a: Average load-loaded end slip curves for No. 8 ASTM A 615 reinforcing bars in a beam-end specimen. RH and RV represent bars with longitudinal ribs oriented horizontally and vertically, respectively (Note: 1 kip = 4.45 kN)
[Darwin and Graham, 1993]

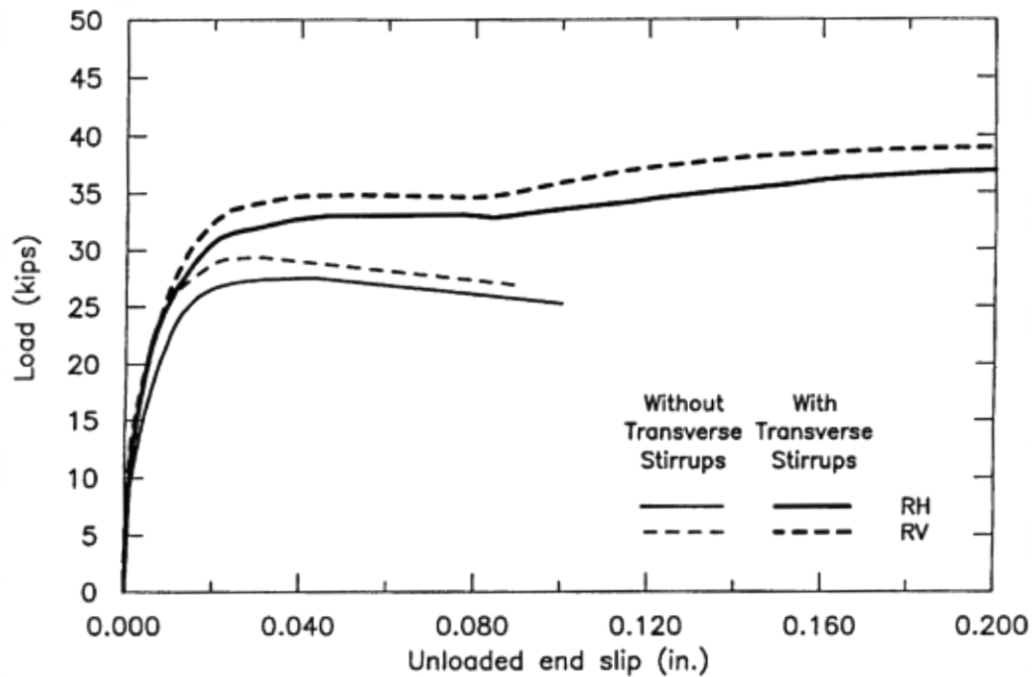


Fig. 2.2b: Average load-unloaded end slip curves for No. 8 ASTM A 615 reinforcing bars in a beam-end specimen. RH and RV represent bars with longitudinal ribs oriented horizontally and vertically, respectively (Note: 1 kip = 4.45 kN)
[Darwin and Graham, 1993]

A bond stress versus slip curve for a bar loaded monotonically and failing by pull-out is shown in Fig. 2.3, *Eligehausen, Popov, and Bertero (1983)*. Bond force and bond stress-slip curves, like bond strength, are structural properties that depend on both the geometry of the bar and the details of the concrete member, including the cover, transverse reinforcement, and state of stress in the concrete surrounding the reinforcement. As shown in Figs. 2.2 and 2.3, bond force and bond stress-slip curves are initially very steep because of adhesion.

Because of concrete shrinkage, which is restrained by the reinforcing bar, small internal cracks exist immediately adjacent to the reinforcing bar. These cracks can act as stress raisers and points of crack initiation at the bar ribs at relatively low loads. Because cracks tend to form in front of the ribs, small splitting cracks may begin to propagate from the ribs. If the reinforcing bar is placed in tension from a free surface, such as a beam-end specimen, it is possible for the crack to propagate to the surface, separating a roughly conical region of concrete from the rest of the specimen.

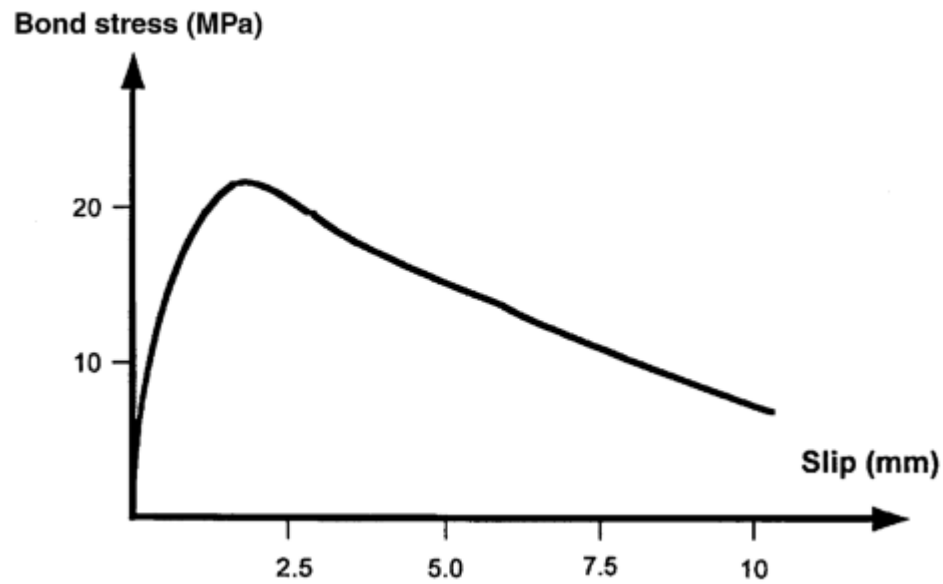


Fig. 2.3: Bond stress-slip curve for bar loaded monotonically and failing by pull-out (Note: 1 MPa = 145 psi)
[Eligehausen, Popov, and Bertero, 1983]

2.3 Factors Affecting Concrete Rebar Bond Strength

The theory of reinforced concrete is based mainly on the bond transferred between the steel bar and the surrounding concrete. This transfer is made possible by the resistance to relative motion or slippage between the concrete and the surface of the embedded steel bar. Several factors affect this relative motion resistance, some are related to the steel bar and others are related to the concrete.

2.3.1 Geometry & Shape

David (1941) studied the effect of different bar geometry on bond stress. This study found that the stress transmission from the loaded end to the free end was higher in case of plain bars than that of ribbed bars. Also, he observed that the stress in the ribbed steel bar was higher near the loaded end than that of plain bars, and this may be attributed to the increase of bond resistance due to the ribs action, which is not available in plain bars.



Another study was conducted by *Maslehuddin et al. (1990)* to evaluate the surface conditions of steel bar on the bond between the reinforcing bar and the concrete. This study succeeded to investigate the effect of different rust degrees on the surface of the steel bar and their corresponding effect on bond with concrete. The results indicated that the 16 mm diameter bar showed no change in bond with concrete, whereas the 32 mm diameter bar showed a slight increasing in bond with concrete. This was attributed to the smaller bar diameters which showed some filling of rust between the lugs, and thus producing a plain surface effect compared to the ribbed bars, while in bigger diameters the increase of the roughness due atmospheric exposure and rust formation, slightly increased the bond.

2.3.2 Rib Angle

Lutz, Gergely and winter (1966) stated that for ribbed bars with face angle of 90 degrees with the axis of the bar, all of the bond strength would be produced by the direct bearing of the rib against the concrete key. In this case, friction between the concrete and steel would be unnecessary, on the other hand bars with 90 degrees angle could have insufficient compaction of the concrete in front of the rib which oppositely affects the bond strength. However, for face angle of zero degree (plain bars), friction caused by adhesion between the concrete and steel would be the only bond component, and loss of this adhesion would destroy the bond completely. As the rib face angle becomes larger, the contribution of the friction component parallel to the face of the rib to the bond becomes smaller and that related to the bearing increases.

Researches done by *Lutz and Gergely* from 1967 to 1970 using pull out test samples showed that bars with rib face angles larger than 45 degrees slipped mainly by compression and crushing of concrete in front of the ribs, on the other hand, bars with rib face angles smaller than 45 degrees slipped mainly by a sliding movement.

Fig. 2.4 shows the variation in rib face angle from 30 to 75, with the bond stress and the corresponding slips. At slips 0.01 and 0.1 mm, the bond stress slightly increases with the increase in the rib face angle. At failure load (slip 1 mm), the bond stress increases with the increase of rib angle from 30 to about 55 or 60. *Carins and*



Abdullah (1994) attributed this to the increase of bearing force due to the increase of bearing area. Also they showed that the large increase in the rib face angle can result in an insufficient concrete compaction below the rib and this factor should be taken into consideration to design the rib face angle.

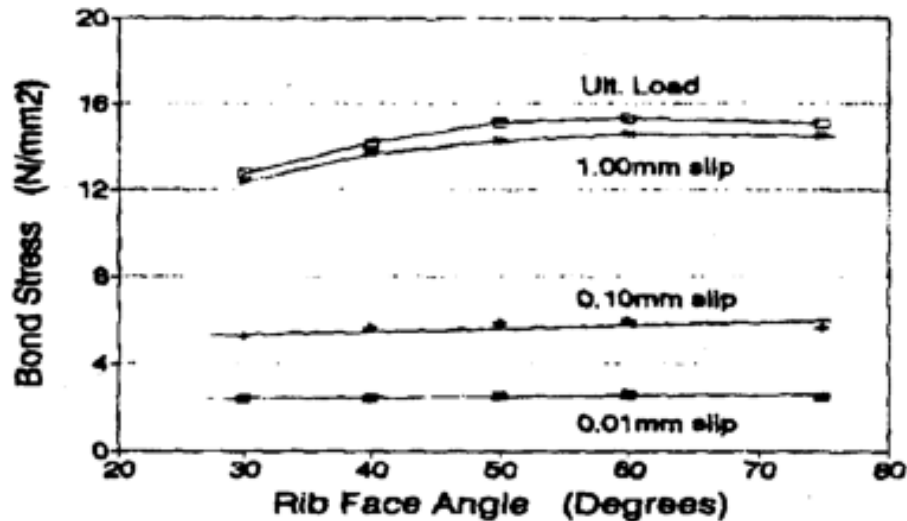


Fig. 2.4: Variation in bond stress with rib face angle
[Cairns and Abdullah, 1994]

2.3.3 Rib Spacing and Rib Height

Abrams (1913) was the first to study the effect of deformations on bond between steel and concrete. He concluded that the ribs had little effect up to an end slip of 0.010 inch, after which the ribs became effective in taking bond stress. He suggested that the rib height should be 1/10 of the bar diameter and spaced 1/2 bar diameter apart. Also the plane of the bearing faces of the ribs should be as close as possible to 90 degrees from the longitudinal axis of the bar.

Clark (1939) found that the greater the bearing rib angle, the better was the bond resistance. A maximum ratio of the shearing to bearing areas of 5 or 6 was desirable for good bond behavior. In the period from 1946 to 1949, *Clark* investigated 17 commercial deformation patterns using pull-out and beam tests. This study found that the bond performance improved for bars with lower ratios of shearing area to

bearing area and recommended that the ratio of shearing area to bearing area be limited to a maximum of 10.

Previous bond studies made by *Rehm (1961)*; *Lutz, Gergely and Winter (1966)*; concluded that the increase in the height of the rib and decrease in the spacing between ribs; would increase rib bearing area to rib shearing area ratio and would improve the bond performance. The ratio of rib bearing area to rib shearing area is called the relative rib area (R_r) which is defined as the ratio of the projected rib area (normal to bar axis) to the product of the nominal bar perimeter by the center to center rib spacing (Fig. 2.5).

$$R_r = \frac{\text{Projected rib area normal to bar axis}}{\text{Nominal bar perimeter} \times \text{Center to center rib spacing}} \quad 2 - 1$$

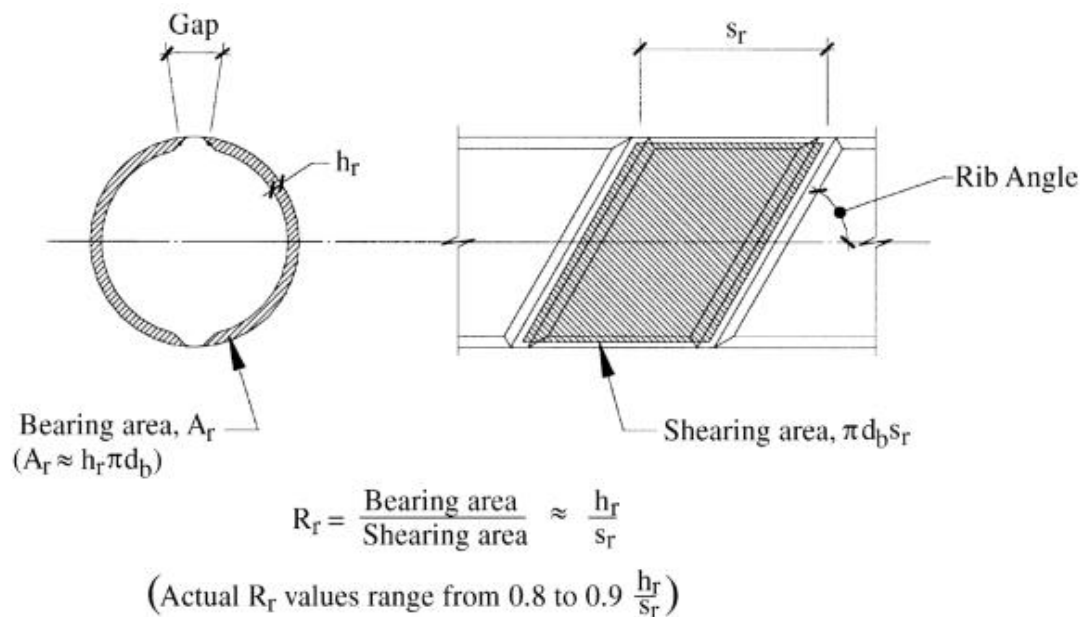


Fig. 2.5: Definition of R_r
 [ACI 408.3R]

Sortez and Holzenbein (1979) suggested a minimum rib height of 3/100 diameter for delaying the onset of splitting. As rib height is reduced, rib spacing must be reduced appropriately. They reported that the variation of rib angle with respect to bar axis from 45 to 90 degrees improved bond performance slightly.



Murata and kawai (1984) studied the bond strength between concrete and Japanese specially machined deformed bars. Test specimens were produced by modifying deformed bars (32 mm diameter) to obtain varying rib spacing ($0.5d - 3.0d$), rib height (1.0, 1.5, 2.0 and 2.5mm) and rib face angles (15 to 90 degrees in 5 degrees increments). This study also included the investigation of the bond characteristics of five different kinds of commercial deformed bars of varying diameters (16 to 57 mm diameter). Conclusions taken from this study were:

- 1- The splitting bond strength increased with the rib face angle up to 45 degrees and showed constant values for rib face angles of 45 degrees or more (Fig. 2.6).
- 2- The splitting bond strength was approximately constant when the rib spacing was less than the bar diameter, but decreased when spacing more than one bar diameter was used (Fig. 2.7).
- 3- The splitting bond strength increased almost linearly with the rib height for rib heights up to 8 % of the bar diameter (Fig. 2.8).

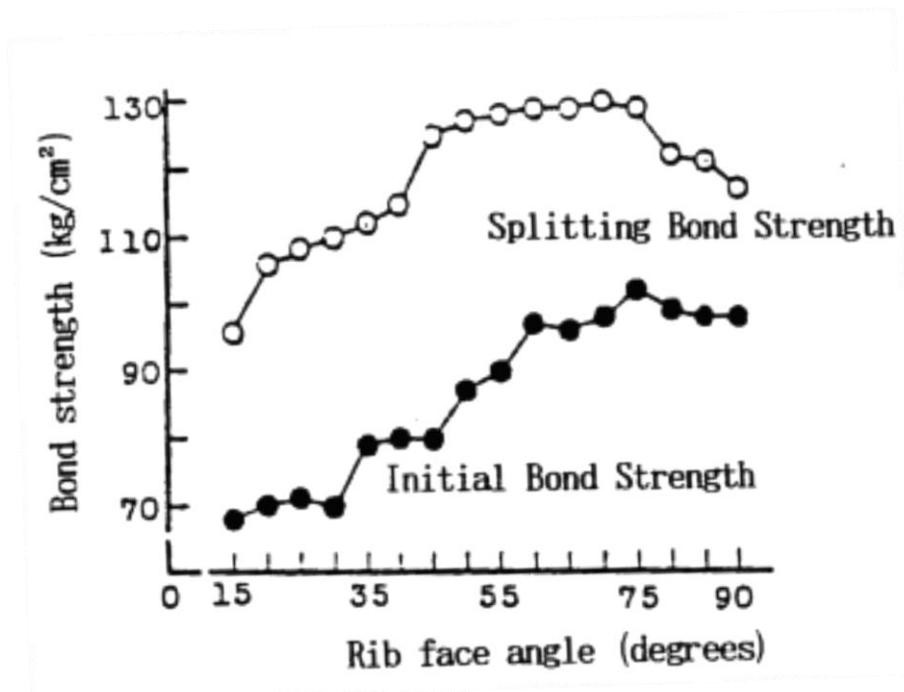


Fig. 2.6: Effect of rib face angle
[Murata and kawai, 1984]

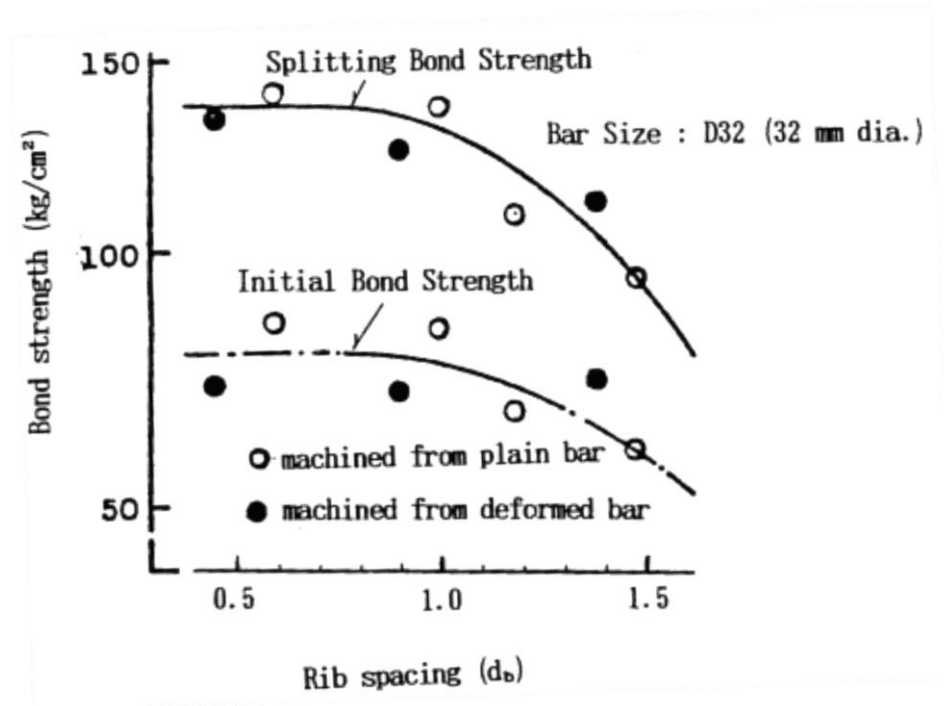


Fig. 2.7: Effect of rib spacing
 [Murata and kawai, 1984]

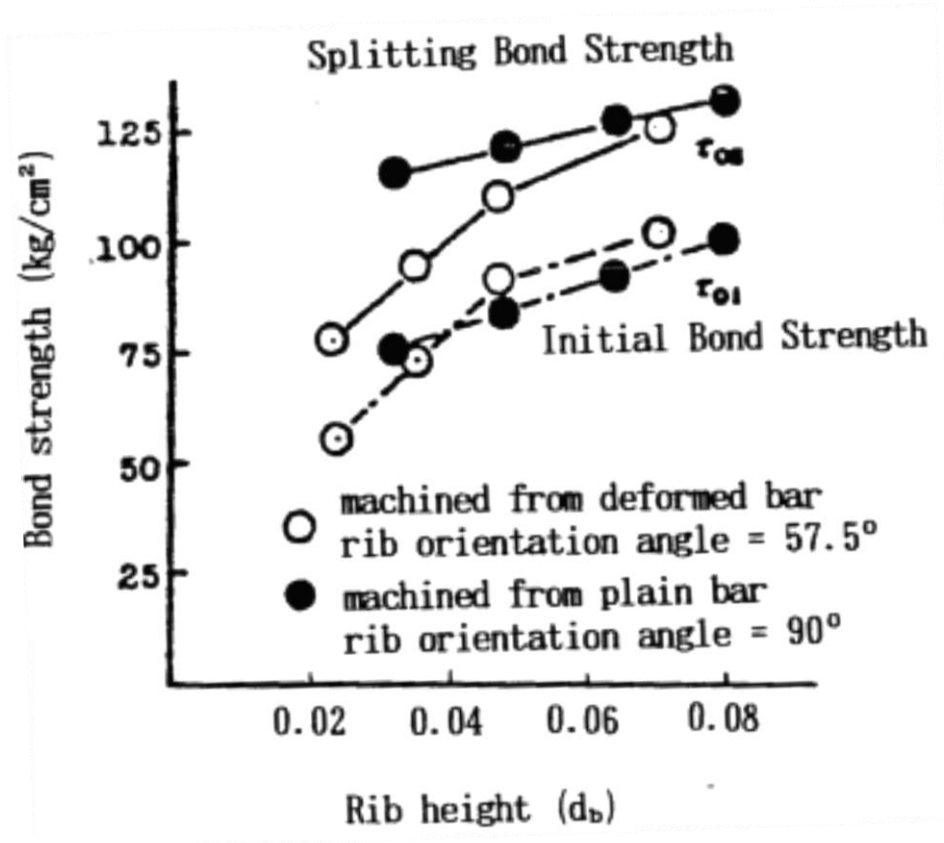


Fig. 2.8: Effect of rib height
 [Murata and kawai, 1984]



Another study was made by *Kokubu and Okamura* using 51 mm diameter bars made of cast iron. Twenty four different deformations patterns shown in Fig. 2.9 were used. The test results indicated that:

- 1- The effect of rib orientation angle was very small within a range from 46 to 90 degrees. Also the effect of rib face angle was small when the angle was 45 degrees or more.
- 2- Bond characteristics between deformed bars and surrounding concrete were affected primarily by three factors: rib height, rib spacing and rib projection length. A bearing area coefficient (BA^*) was calculated which include all three factors and well describe bond characteristics as shown in Fig. 2.10.

$$BA^* = \frac{\text{Rib height} \times \text{Rib projection length}}{\text{Rib spacing} \times \text{Nominal perimeter}} \quad 2 - 2$$

$$\text{Rib height} \leq 0.2 \text{ Rib spacing}$$

A BA^* of more than 0.1 is needed for large deformed bars. Bond strength increased as rib clear spacing decreased and as rib height increased. But if the ratio of rib height to rib clear spacing is too large, the shear capacity of concrete between ribs will decline because of a decrease in the interlocking effect of aggregate. Therefore, for large deformed bars, the effective rib height was 20 % of the rib clear spacing.

- 3- Crack widths in RC beams using large deformed bars which produced good bond performance in pullout tests, hardly increased during repeated loading.
- 4- Bars with rounded intersections between the ribs and the bar have better fatigue life because the stress concentrations are reduced. However, all large deformed bars showed less fatigue resistance than normal deformed bars.

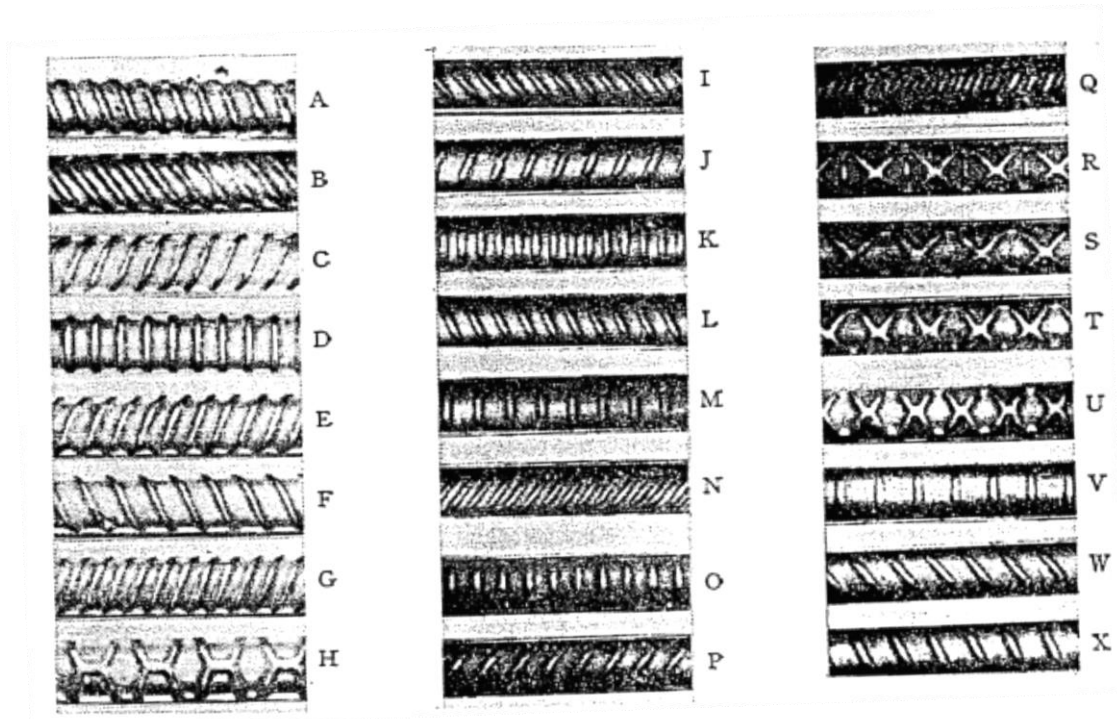


Fig. 2.9: Deformation patterns of bars for pullout test
 [Kokubu & Okamura, 1977]

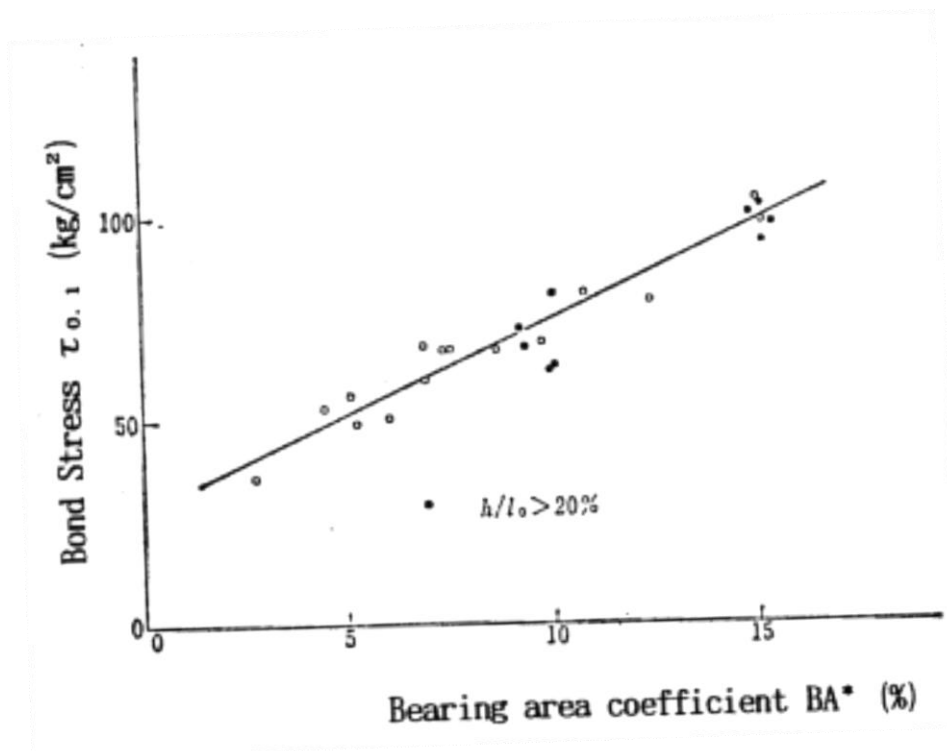


Fig. 2.10: Relationship between BA* and bond stress
 [Kokubu & Okamura, 1977]

In 1991, *Akasi, Fujii* and *Morita* conducted two types of pullout tests as shown in Fig. 2.11. Specimens of Series 1 were 225 mm cubes with a steel bar positioned at the center. Specimens of Series 2 were identical to Series 1 except that the cubes were placed in steel tubes. The bars had varying rib geometries. Two rib heights (h) of 2.5 and 1.3 mm, and three rib spacing (l) of 25.4, 17.8 and 10.2 mm. Specimens with three different concrete strengths (300 kg/cm^2 , 600 kg/cm^2 and 900 kg/cm^2) were cast for each series. The test results are summarized as follows:

- 1- The stiffness and the bond strength at splitting as indicated by bond-slip curves increased with concrete strength (Fig. 2.12).
- 2- Maximum shear strength under sufficient confinement to prevent splitting is proportional to the 0.85 power of concrete strength (Fig. 2.13).
- 3- The concrete strain perpendicular to the bar axis at a given bond stress increased as h/l decreased.

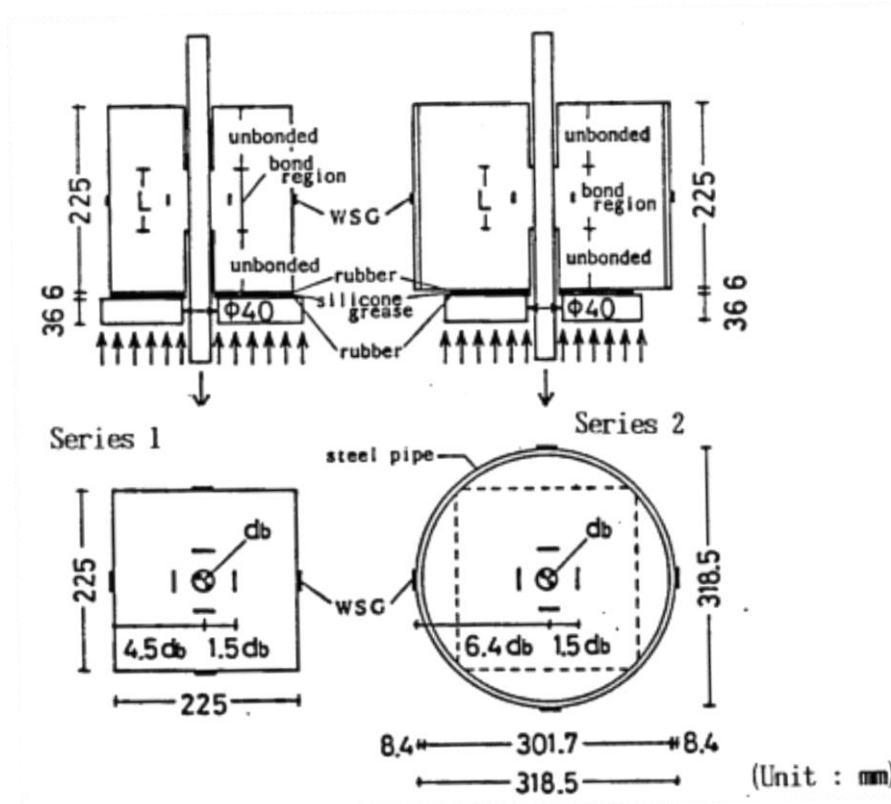


Fig. 2.11: Details of specimens
 [Akasi, Fujii & Morita, 1991]

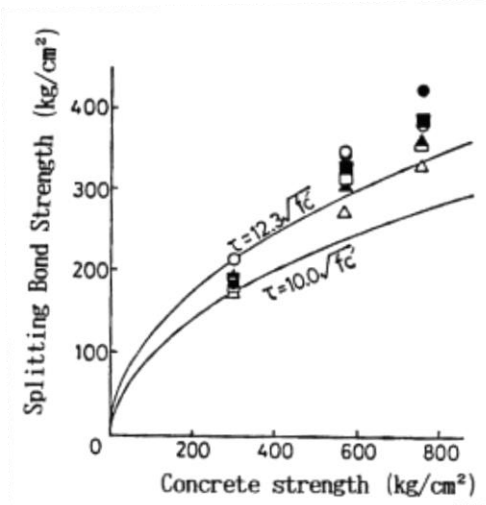


Fig. 2.12: Effect of concrete strength on bond strength at splitting
 [Akasi, Fujii & Morita, 1991]

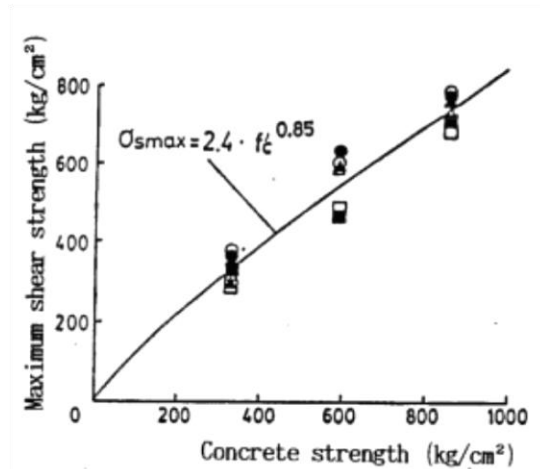


Fig. 2.13: Relation between maximum shear strength and concrete strength
 [Akasi, Fujii & Morita, 1991]

2.3.4 Casting Position and Concrete Confinement

Park and Paulay (1975) showed that the bond-slip relationship for deformed bars is primarily affected by the quality of the concrete in front of the bar ribs. The quality of concrete in this region depends on its relative position of casting. Fig. 2.14 shows the effect of different casting position on the bond-slip relationship. Soft and spongy layer of concrete can be formed under the ribs in case of casting perpendicular to the bar length. This results in a higher slip (compared to the other casting positions) due to the crushing of the weak concrete under the ribs.

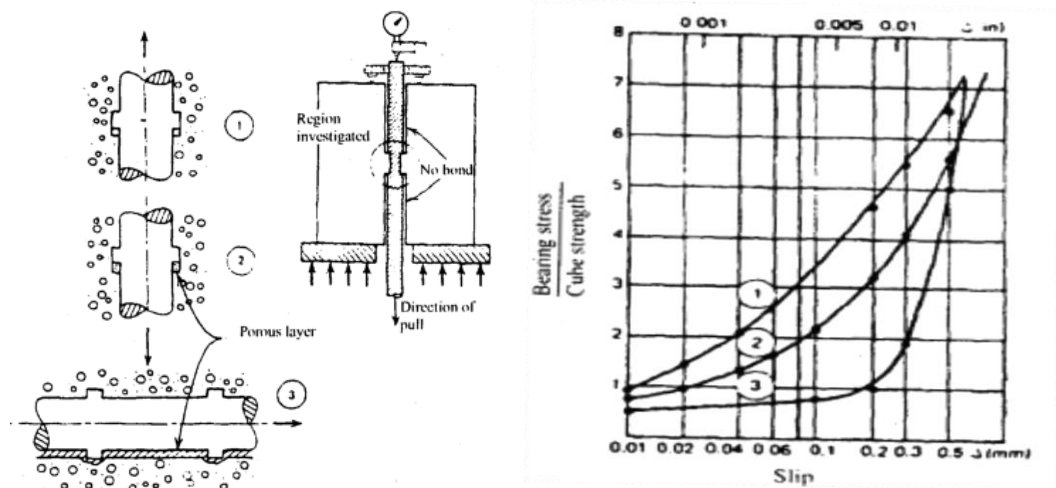


Fig. 2.14: The influence of casting position on bond performance (Deformed bars)



Also this study investigated the concrete quality effect on bond-slip relationship for plain bars. Fig. 2.15 shows the effect of casting position for 16mm plain bars. The upper curves of each pair in the figure were obtained for heavily rusted and pitted bars. The lower curves of each pair are for smooth surface bars. The ultimate bond strength is drastically reduced in the case of horizontal bars as compared with vertical bars. Also it is expected that the top bars in a beam will have poorer bond characteristics than the bottom bars, since the water and air gain will be greater under top bars. In addition, the relative downward movement of the surrounding concrete caused by settlement of the fresh mixture can be large.

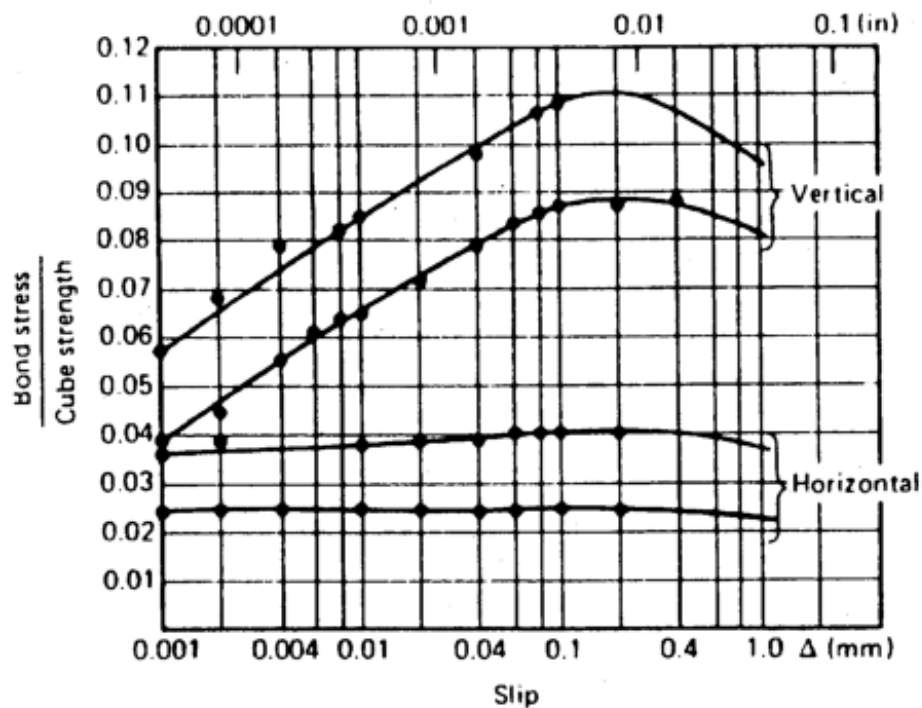


Fig. 2.15: Bond-slip relationship for 16mm plain rounded bars in different casting positions
 [Park and Paulay, 1975]

In 1967 *Welch* and *Patten* compared the bond performance between top and bottom bars in concrete casted in both leaky timber moulds and in well-sealed steel moulds. Fig. 2.16 demonstrates their results, the upper two curves indicate to the well-sealed steel moulds for top and bottom bars and the lower part indicates to the leaky timber mould placing for the same bars. This shows the effect of concrete settlement on bond, particularly for top bars. The ACI code recognizes this phenomenon by requiring 40% excess development length for top-cast deformed bars.

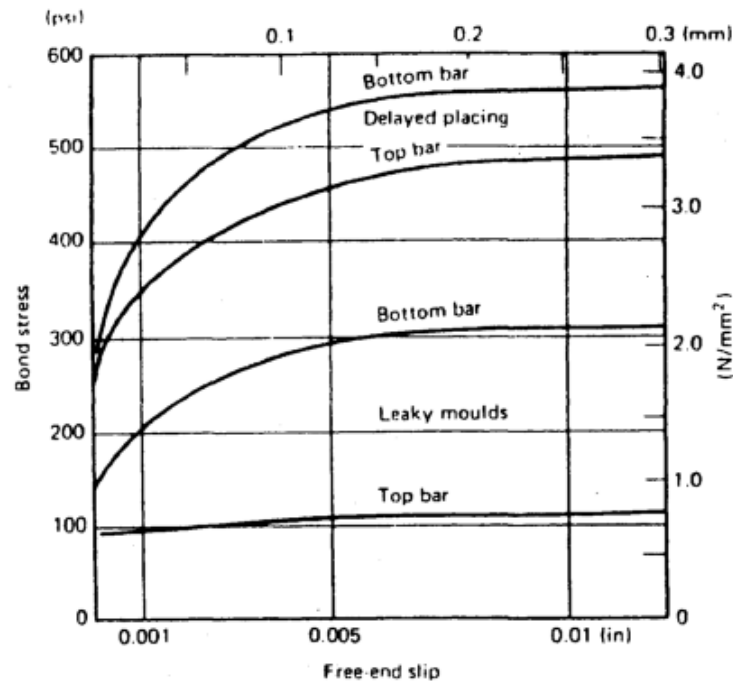


Fig. 2.16: Bond-slip relationship for plain rounded bars as affected by settlement of fresh concrete

The widening of splitting cracks can be restricted if the concrete that surrounds a bar is confined in certain areas, such as at the simply supported ends of beams, transverse compression is normally available from the reaction force. Transverse compression is beneficial to the anchorage of reinforcement.

Increased concrete cover has been found to produce some increase in the resistance against splitting however, the improved bond performance is not proportional to the additional cover thickness. For large size bars, the beneficial effect is not very significant. For these bars, as a rule, the effect on the formation and widths of cracks under service loading conditions is the governing criterion in selecting an appropriate value for allowable average bond stress. Extra cover does not provide protection against excessive surface crack width; however, medium sized top bars appear to benefit more from added cover.

Stirrups, particularly when closely spaced, prevent the opening of cracks that form along the embedded bars and enable greater bond forces to be transmitted. In many situations, this is only possible if the shearing stresses are transmitted across splitting cracks by means of aggregate interlock.



The aim of confinement by means of stirrups or transverse reinforcement is to prevent a failure along a potential splitting crack and to enforce, if necessary, a shear failure, which is associated with the maximum attainable bond strength, *Welch and Patten (1967)*.

2.3.5 Concrete Cover and Bar spacing

Bond force-slip curves become steeper and bond strength increases as cover and bar spacing increase. The mode of failure also depends on cover and bar spacing (*Untrauer 1965, Tepfers 1973, Orangun, Jirsa, and Breen 1977, Eligehausen 1979, Darwin et al. 1966*). For large cover and bar spacing, it is possible to obtain a pull-out failure. For smaller cover and bar spacing, a splitting tensile failure occurs, resulting in lower bond strength. The latter failure mode is the type expected to govern for most structural members. Splitting failures can occur between the bars, between the bars and the free surface, or both. Pull-out like failures can occur with some splitting if the member has significant transverse reinforcement to confine the anchored steel, *ACI Committee 408*.

2.3.6 Development and Splice Length

Increasing the development or splice length of a reinforcing bar will increase its bond capacity. The nature of bond failure, however, results in an increase in strength that is not proportional to the increase in bonded length. The explanation starts with the observations that bond forces are not uniform (Fig. 2.17) and that bond failures tend to be incremental, starting in the region of the highest bond force per unit length.

According to the *ACI Committee 408*, in the case of anchored bars; longitudinal splitting of the concrete initiates at a free surface or transverse flexural crack where the bar is most highly stressed. For spliced bars, splitting starts at the ends of the splice, moving towards the center. For normal strength concrete, splitting may also be accompanied by crushing of the concrete in front of the ribs as the bar moves with respect to the concrete. For higher strength concrete and for normal strength concrete

in which the bars are epoxy coated, the degree of crushing in front of the ribs is significantly decreased.

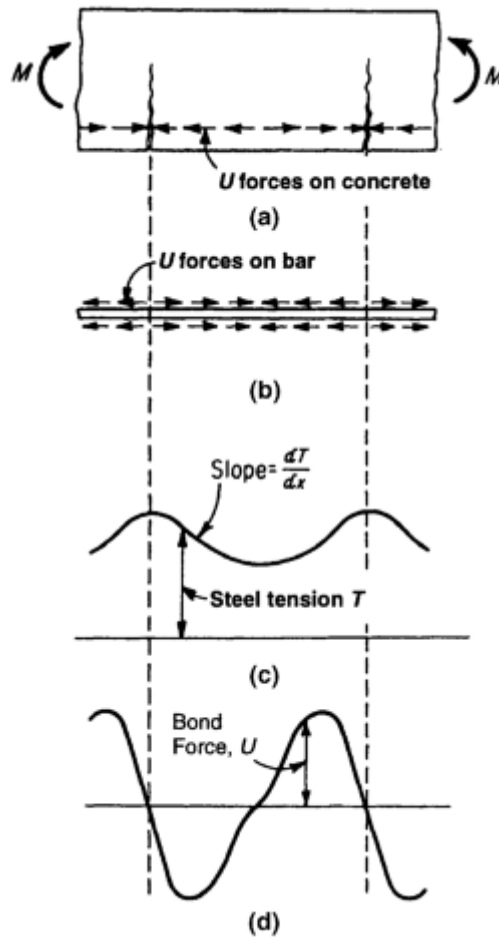


Fig. 2.17: Variation of steel and bond forces in reinforced concrete member subjected to pure bending: (a) cracked concrete segment. (b) Bond stresses acting on reinforcing bar. (c) Variation of tensile force in steel. (d) Variation of bond force along bar.

[Nilson et al., 2004]

2.3.7 Steel Stress and Yield Strength

For a number of years, concern existed that bars that yielded before bond failure produced average bond stresses significantly lower than higher strength steel in similar test specimens that did not yield (Orangun, Jirsa, and Breen 1975). As a result, test specimens were often deliberately configured to ensure that the bars did not yield prior to bond failure.



As it turns out, the bond strengths of bars that yield average only about 2% less when not confined by transverse reinforcement and about 10% greater when confined by transverse reinforcement than similar bars with the same bonded lengths made of higher strength steel that does not yield (*Darwin et al. 1966, Zuo and Darwin 1998, 2000*).

2.3.8 Aggregate Type and Quantity

For bars not confined by transverse reinforcement, *Zuo and Darwin (1988, 2000)* observed that a higher strength coarse aggregate (basalt) increased concrete tensile strength by up to 13% compared with a weaker coarse aggregate (limestone). This observation was explained based on studies using the same materials (*Kozul and Darwin 1997, Barham and Darwin 1999*) that showed that concrete containing the basalt had only slightly higher flexural strengths, but significantly higher fracture energies (more than two times higher) than concrete of similar compressive strength containing limestone for compressive strengths between 20 and 96 MPa. The higher fracture energy provided by the basalt resulted in increased resistance to crack propagation, which delays splitting failure and increases bond strength. *Zuo and Darwin* observed no effect of coarse aggregate quantity on concrete tensile strength.

2.4 Bond Failure Modes

Many scientists, who have contributed to the knowledge of the many aspects of bond (*Task group bond model, 2000*), agree that the interaction between the concrete and the bar subjected to a tensile force is characterized by four different stages (Fig. 2.18), these stages are:

- Stage I (Un-cracked stage)
- Stage II (Micro-cracks)
- Stage III (Splitting cracking)
- Stage IVa (Bond failure of plain bars)
- Stage IVb (Bond failure of deformed bars surrounded by light confinement)
- Stage IVc (Bond failure of deformed bars surrounded by heavy confinement)



2.4.1 Un-Cracked Stage

At this stage, the bond stress (τ) is less than the maximum bond stress (τ_1^{PS}). τ_1^{PS} is defined as the maximum bond stress that the plain bar can resist without slipping. Here chemical adhesion is responsible for the bond efficiency and no bar slip occurs, however localized stress occurs close to the lug tips. τ_1^{PS} ranging from 1.0 to 2.0 MPa is appropriate for the analysis of the bond between deformed bars and concrete *Choi & Lee (2002)*. However, the *ACI committee 408 (1991)* suggested that the bond strength due to adhesion is between 0.48 and 1.03 MPa.

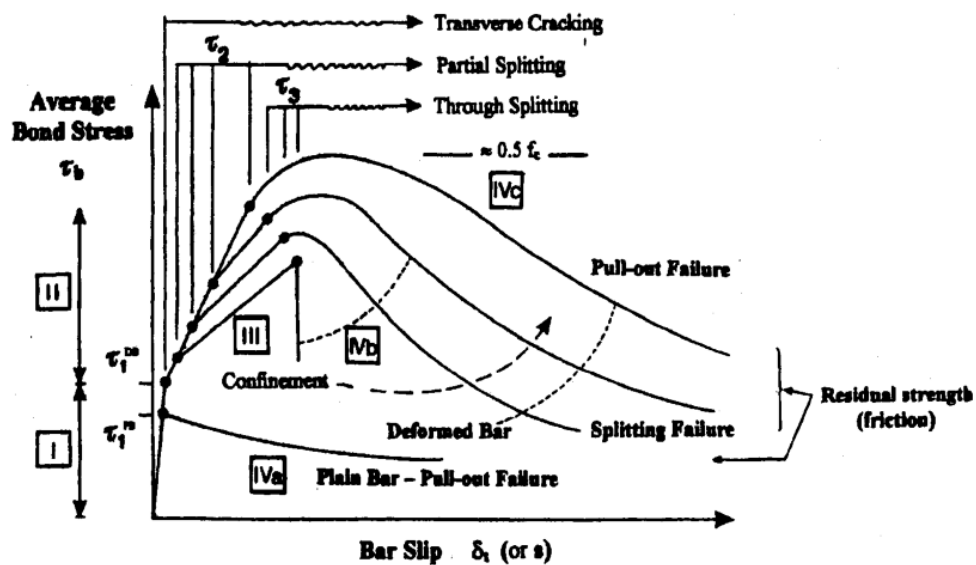


Fig. 2.18: Local bond stress-slip law
 [Task group bond model, 2000]

Cairns & Abdulla (1994) studied the adhesion between the concrete and steel plates. Specimens were cast in which the concrete was sandwiched between two plates of steel and two plates of steel with epoxy coating. They observed minimal adhesion in the case of coated plates, and the coated plates were noted to be clean after failure, while the un-coated plates were covered with a layer of crushed mortar.

2.4.2 Micro-cracks

The maximum bond stress that the deformed bar can resist without occurring a transverse micro-cracks is defined as τ_1^{DS} . At this stage, the bond stress (τ) is higher

than (τ_1^{Ds}) . The chemical adhesion breaks down at this stage, the lugs induce large bearing stresses in the concrete p^* (defined as the reaction of the bar lugs bearing against the concrete) (Fig. 2.19a) and transverse micro-cracks originate at the tips of the lugs as well as compressing of the porous concrete in front of the lug (in some cases due to lack of compaction) allowing the bar to slip, but the wedging action of the lugs remain limited and there is no concrete splitting (Fig. 2.19b).

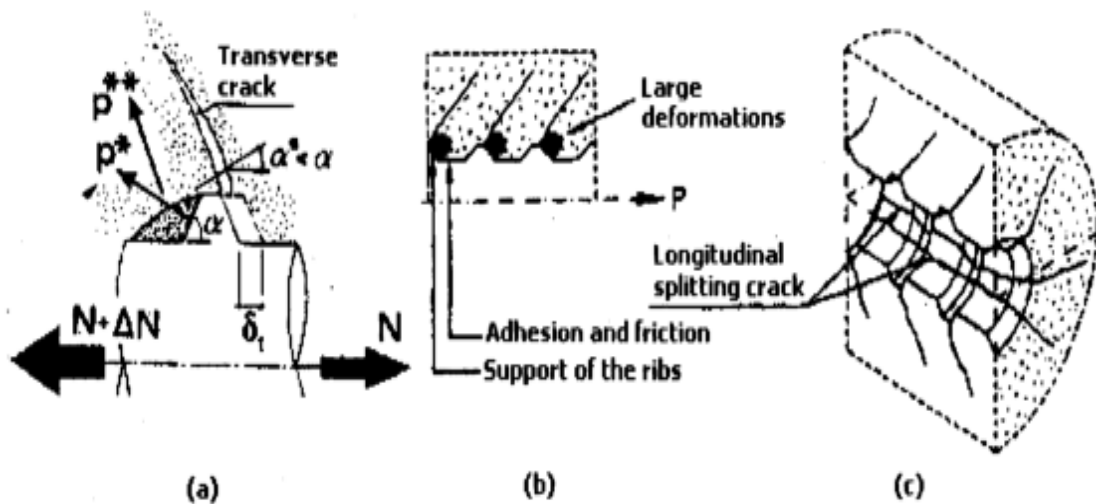


Fig. 2.19: (a) Bar-concrete slipping and wedging action of the bar. (b) Friction & bearing action. (c) Transverse cracking and splitting [Task group bond model, 2000]

2.4.3 Splitting Cracks

At this stage, when continuous increase of bond stress takes place, the longitudinal cracks (splitting cracks) spread radially, owing to the wedging action, which is enhanced by the concrete crushing in front of the lugs as shown in Fig. 2.19c.

It was observed by *Rehm* (1968) that the slip resistance upon reloading is considerably higher than the slip resistance found initially. This was attributed to the ribs that are bearing against the compacted non-porous crushed concrete at the second loading compared with the porous intact concrete during the initial loading (Fig. 2.20).

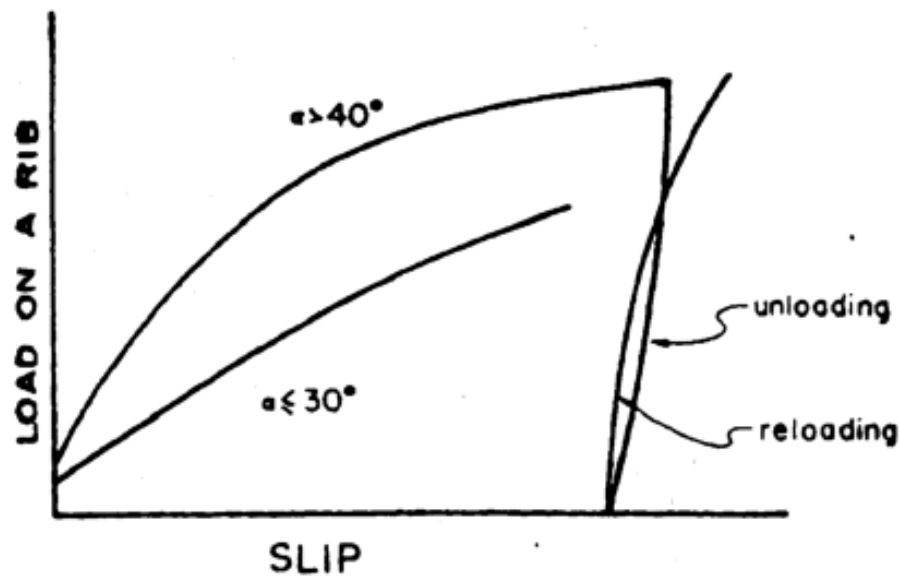


Fig. 2.20: Load slip curve for cyclic loading with different rib angles
[Rehm, 1968]

2.4.4 Bond Failure of Plain Bars

In the case of plain bars, the bond resistance is assumed to be chemical adhesion between the mortar paste and the bar surface, however, low stresses will cause sufficient slip to break the adhesion between the concrete and the steel. Once slip occurs, further bond resistance is developed only by friction and by the wedging action of small dislodged sand particles between the bar and the surrounding concrete. Failure occurs when the adhesion and friction resistance is overcome, and the bars usually pull out from the encasing concrete.

2.4.5 Bond Failure of Deformed Bars Surrounded by Light Confinement

The bond in this stage tends to fail abruptly in the case of deformed bars surrounded by light confinement; the longitudinal cracks accompanied by slip on the rib face break out through the entire cover thickness (Fig. 2.21c).

In the case of sufficient amount of transverse reinforcement (medium confinement) is provided, a longitudinal cracks accompanied by crushing or shearing-



off in the concrete below the ribs will occur through the entire cover thickness (Fig. 2.21b). The bond stress values as high as $(1/3 - 1/2) f_c$ can be developed during this stage, with the unavoidable and often unacceptable side-effect represented by very high slip values.

2.4.6 Bond Failure of Deformed Bars Surrounded by Heavy Confinement

In the case of deformed bars surrounded by heavy confinement, splitting doesn't occur and bond failure is caused by bar pull out. The force transfer mechanism changes from rib bearing to friction along the vertical line between the tops of the ribs (Fig. 2.21a). Under continued loading, the interface is smoothed due to wear and compaction, leading to a further decrease of bond resistance.

As far as Stage III is concerned, due to the build-up of the wedging action exerted by the bars and to the propagation of the splitting cracks, all possible contribution to the confinement are mobilized. In fact, the confinement efficiency depends on the concrete cover thickness, bar spacing, reinforcement, and transverse pressure (Ferguson, 1966; Edwards & Jannopoulos, 1978; Morita & Kaku, 1979).

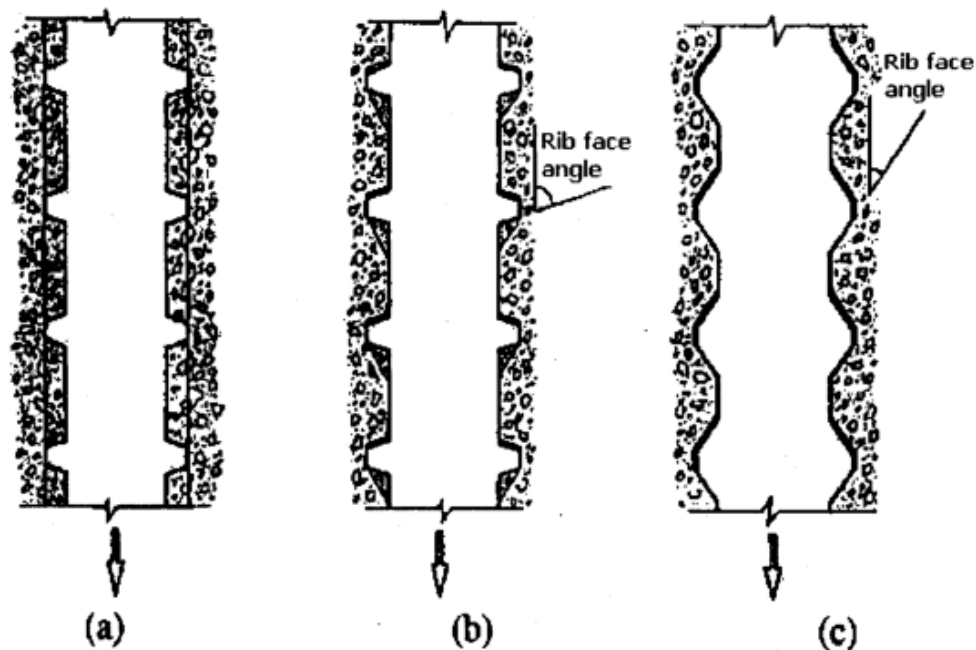


Fig. 2.21: Modes of bond failure: (a) Heavy confinement pull-out. (b) Medium Confinement, splitting induced pull-out accompanied by crushing and/or shear-off in the concrete below the ribs. (c) Light confinement splitting accompanied by slip on the rib face [Task group bond model, 2000]



2.4.7 The ACI Committee 408 Failure Modes

According to the *ACI*, the forces on the bar surface are balanced by compressive and shear stresses on the concrete contact surfaces, which are resolved into tensile stresses that can result in cracking in planes that are both perpendicular and parallel to the reinforcement, as shown in Figs. 2.22a and 2.22b. The cracks shown in Fig. 2.22a, known as Goto (1971) cracks, can result in the formation of a conical failure surface for bars that project from concrete and are placed in tension. These cracks otherwise play only a minor role in the anchorage and development of reinforcement. The transverse cracks shown in Fig. 2.22b form if the concrete cover or the spacing between bars is sufficiently small, leading to splitting cracks, as shown in Fig. 2.22c. If the concrete cover, bar spacing, or transverse reinforcement is sufficient to prevent or delay a splitting failure, the system will fail by shearing along a surface at the top of the ribs around the bars, resulting in a “pull-out” failure, as shown in Fig. 2.22d.

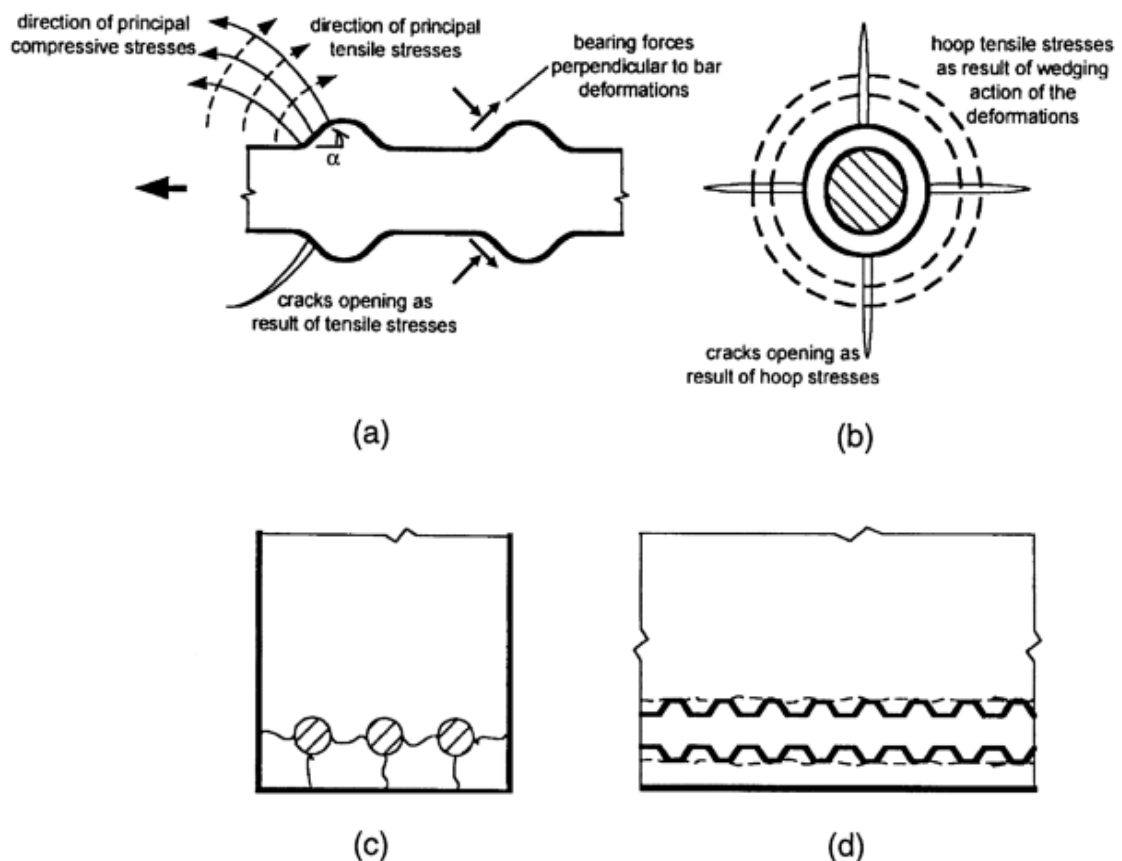


Fig. 2.22: Cracking and damage mechanisms in bond: (a) Side view of a deformed bar with deformation face angle α showing formation of Goto (1971) cracks. (b) End view showing formation of splitting cracks parallel to the bar. (c) End view of a member showing splitting cracks between bars and through the concrete cover. (d) Side view of a member showing shear and/or local concrete crushing due to bar pull-out. [*ACI Committee 408*]



Mechanisms of Steel Corrosion

3.1 Introduction

“It has always been stated that the combination of concrete and reinforcing steel is an optimal one not only because of the mechanical performance but also from the point of view of long-term performance. Concrete is a durable material, much more than steel and the encasement of steel in it provides the steel with a protective environment and allows it to function effectively as reinforcement. Theoretically, this combination should be highly durable, as the concrete cover over the steel provides a chemical and physical protection barrier to the steel, and can potentially eliminate steel corrosion problems which occur readily in bare steel structures.” *A. Bentur, S. Diamond and N.S Berke.*

Good quality concrete provides a high alkaline environment for steel reinforcement, and this is due to the products of the cement hydration process. The outcomes of this process are hydroxides of sodium, potassium and calcium. Hydrated or dehydrated surface oxide films which are formed in this oxidative environment play a major role in inhibiting the against corrosion of iron and steel. The passive films formed on pure iron are not so stable and consequently the passivation state of iron is not maintained for prolonged time periods. However, chromium alloys like stainless steels exhibit stable passivation which is maintained for long time periods even under non-oxidative environments, *Toshiaki (2005).*

As mentioned before in the previous chapters, ASTM defined corrosion as the chemical or electrochemical reaction between a metal and its environment that produces a deterioration of the material and its properties. It is very important to study the structure of corrosion products, since the corrosion rate of steel is known to depend strongly on the condition of such corrosion products covering the surface as a protective film. Life time of steel is sometimes dominated by environmental degradation, so that the structure of corrosion products formed on the surface of steel during exposure to air for a prolonged period is of great importance.



3.2 Passivation Oxide Films on Iron

Passivation films on iron have been studied by some researchers with regard to thickness and physical properties. Passivation films can be formed by one of these two methods; electrochemical or chemical. The two methods are assumed to be the same, since the two methods need an oxidative condition. This condition can be induced by high anodic electrode potential or a strongly oxidative agency.

Fig. 3.1 shows the thickness-anodic potential relation of the passivation film. The film formation was measured in different solutions with different pH values, and the current density taken during oxidation is also plotted. From the figure, it is obvious that the thickness of the passivation film increases linearly with increase of potential and the current density is kept almost constant in the passive potential region, depending on the solution pH.

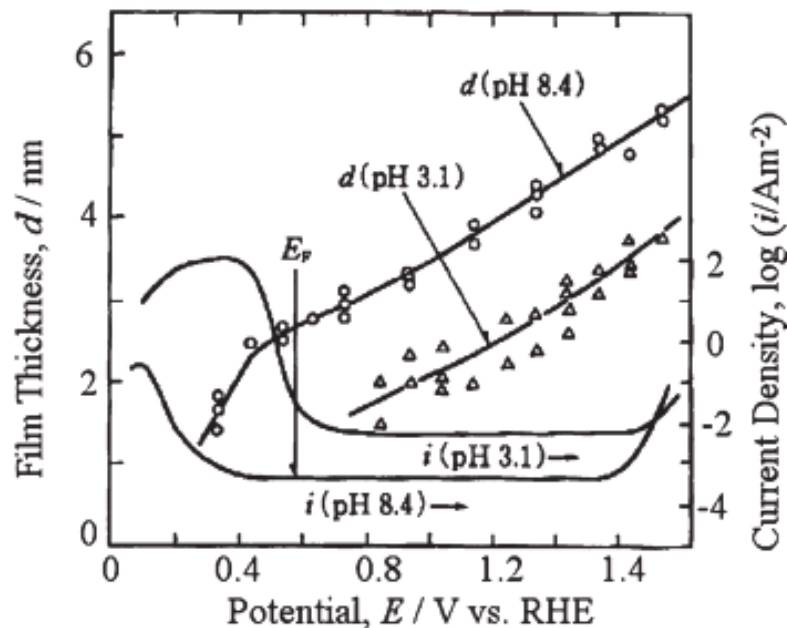


Fig. 3.1: Film thickness-potential and current density

[*Characterization of corrosion products, 2005*]

The pore fluid in a concrete matrix is the electrolyte for reinforcement corrosion. The high alkalinity of the pore fluid in normal concretes provides passivity



to steel reinforcement against corrosion. The high pH (about 13) of concrete pore water solution results in the formation and maintenance of a passive film (oxide layer) on the surface of the reinforcing steel bar, *Bentur et al. (1997)*. However, this passivity can be broken if the concrete surrounding the reinforcement undergoes carbonation and loses its high pH.

The concrete pore solution consists primarily of KOH and NaOH. Due to the high alkalinity of the concrete pore water, the steel reinforcing bars are passivated by an iron oxide film that protects the steel from corrosion (Fig. 3.2). The oxide film itself is a product of the initial corrosion of the steel reinforcing bar.

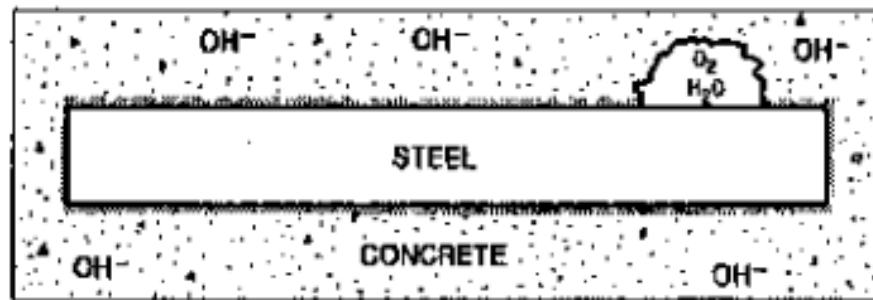


Fig. 3.2: Iron oxide film around the steel bar
[*Materials & Methods for Corrosion Control, 2000*]

3.3 Depassivation of Steel

Durability is a main factor during the design of reinforced concrete structures exposed to marine environments. The service life of a reinforced concrete structure can be divided into an initiation period, during which chloride ions penetrate the concrete cover and initiating corrosion, and a subsequent propagation period during which corrosion leads to a limit state affecting the serviceability or safety of the structure, *Bertolini (2008)*.

In order for corrosion to initiate, the steel reinforcing bar must be depassivated. For depassivation to occur, oxygen, water, and an aggressive ion such as chloride need to be available, and the concrete needs to have low resistivity. The most



important factor for depassivation is the intrusion of chloride ions from the outer environment or from the concrete matrix itself. Possible sources of chloride include:

- Concrete aggregates.
- Mixing water.
- Admixtures (in particular, accelerators).
- Sea water.
- Ground water.

Concrete aggregates quarried from sites associated with sea water or ground water may contain chlorides. If these types of aggregates are used in the concrete manufacturing, it is possible to produce a concrete that already has a chloride concentration at or above the limit for corrosion initiation.

There is no fear of using potable water in concrete although it contains chlorides. Potable water contains small amounts of chlorides (20 to 100 ppm). This amount of chlorides is generally considered to be insignificant, and produce concrete with chloride concentration that is much lower than the threshold limit. Other types of mixing water may contain high amount of chlorides specially sea water.

When using admixtures specially water reducers and accelerators, the amount of chlorides is considered to be insignificant if the chloride content is less than 0.01 percent by mass of the cementitious material, *FHWA*.

Several theories have been presented to explain the role of chloride ions, since the process by which steel reinforcing bars depassivated is not fully understood. Chloride ions reach the steel bars by penetrating the concrete via the pore water and through cracks in the concrete cover. One of the theories, the oxide film theory, states that the chloride ions break down the passive oxide film, and at this point the steel reinforcing bar becomes depassivated and corrosion may be initiated. In the transitory complex theory, chloride ions act as a catalyst. The chloride ions combine with the ferrous ions to form a soluble iron chloride complex that diffuses away from the anode. When carbon dioxide penetrates concrete and dissolves in the pore solution, carbonic acid is formed. This acid reacts with the alkali in the cement to form



carbonates and to lower the pH of the concrete. When the alkalinity reaches a low enough level, the steel reinforcing bar becomes depassivated and, in the presence of sufficient water and oxygen, corrosion is initiated and proceeds.

3.4 Corrosion Initiation on Iron and steel

Corrosion is a natural phenomenon, where a metal tends to transform to its native form which is the natural ore state, often as oxides. This process does not take place individually but it needs a series of electrochemical reactions with the passage of an electric current. Many factors affect the corrosion rate as the type and nature of the metal, the surrounding environment, temperature and other related factors.

The rate of corrosion remains very low as long as the passive film is intact on the reinforcing steel surface. This oxide layer prevents the steel from reaction with oxygen. Steel will remain corrosion resistant in concrete if the concrete cover prevents air and water from reaching the embedded reinforcement, *Jones (1996)*. This problem had led to *American Concrete Institute (ACI)* specifications that require rebar to be entirely encased in concrete, with a minimum concrete cover and spacing between bars. This cover provides limited fireproofing and corrosion resistance to the steel. Significant corrosion does not occur for steel in concrete that is either very dry or continuously saturated because both air and water are necessary for corrosion to be initiated.

Elizabeth Waller simply defined corrosion as the process by which steel releases the energy imparted during the milling process and returns to its pre-milled iron ore state. Some factors are essential for this mechanism to initiate as the presence of water, oxygen, and chloride ions, and is therefore highly dependent on the permeability, electrical resistivity, and temperature of the concrete. ACI code specifies a maximum water/cement ratio of 0.40 for R/C subject to marine environments, since decreasing the water/cement ratio of the concrete mix reduces its permeability and void ratio of the concrete, and therefore reduces the amount of water and oxygen that can be contained within the voids of the concrete. Reducing the



moisture content also reduces the electrical conductivity of the chloride ions in the concrete.

As mentioned before, an electrochemical cell is an essential factor for corrosion to occur. A cell consists of an anode and a cathode, separated by an electrolyte, and connected by a metallic conductor, *Cathodic (1998)*. The anode is the area in which oxidation occurs, or where electrons are released. The cathode is the area where reduction occurs, or where electrons are consumed, *Jones (1996)*. The electrolyte needed for this cell is generally an aqueous solution that can carry ions, such as salt water, or, in concrete, alkaline pore solution, *Cathodic (1998)*. Steel, in reinforced concrete, acts as a cathode when it is in the passive state. When the passive film is lost, parts of the steel act as anode and start to corrode. The passive film can be lost either uniformly by a reduction in the pH of the concrete due to carbonation, or by local breakdown due to chloride ions.

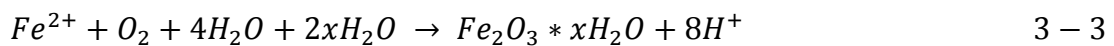
In order for corrosion to take place, chloride ions must first penetrate the concrete to the level of the steel. The period of time required for conduction of the ions is called the “*initiation*” or “*incubation*” stage of the corrosion process. Once this stage happened, stage two of the corrosion process, chemical corrosion, begins. In the presence of water and oxygen steel will form an iron oxide, rust, film around the bar. The chloride ions initiate damaging corrosion by passing through the iron oxide film surrounding the steel and reacting with the iron to form a soluble iron-chloride complex. This complex then diffuses away from the bar and reacts again with the iron to form the ferrous hydroxide, and finally frees the chloride ions to continue corrosion, *Waller (2005)*.

Potential differences between Cathodic and anodic sites within a structure cause current to flow in the pore solution of the concrete, and through the metal reinforcement, *Polder (1998)*. When oxygen is present, as is usually the case, the oxidation and reduction reactions at the steel-concrete interface are, respectively,





The oxygen reacts with water to form hydroxyl, and then reacts with the metal ions to produce a ferrous hydroxide. This reacts with water and oxygen again to further oxidize metal ions and form ferric hydroxide. Through dehydration ferric hydroxide becomes ferric oxide, also known as iron oxide or “rust”, *Waller (2005)*. The corrosion reaction will only continue if there is a cathodic reaction to accept released electrons, so these corrosion reactions can be stopped if oxygen and water are not available at the cathodic sites on the steel, *Bentur et al. (1997)*. Therefore, the total chemical reaction is,



3.5 Critical Chloride Content

There is no effect for chloride-induced corrosion until particular chloride content or “threshold” is reached at the level of steel. According to the Federal Highway Agency (FHWA), the threshold level can be described by the critical chloride content (CCC) as a percent of cement weight or the chloride concentration threshold by concrete volume (lb/yd³ or kg/m³). The FHWA specifies CCC as 0.4 – 1% by cement weight for typical carbon steels. In the presence of higher alkalinity of the concrete and the water in the voids, the iron oxide film protecting the steel from the initiation of chloride corrosion will provide more protection to the steel and increase the corrosion threshold, *Waller (2005)*.

Reinforcing steel bars embedded in concrete depassivated when a certain amount of chlorides reach the bars’ surfaces. The Cl⁻/OH⁻ ratio seems to be the most accurate parameter to take into account when testing the corrosion onset in reinforced concrete, *M. Pourbaix (1973)*. However, due to the difficulty in measuring OH⁻ concentration in concrete, the free and total chloride contents by weight of cement or concrete are the other parameters that have been widely used to indicate the corrosion risk. *Haussmann and Gouda* were the first in identifying the mean value of Cl⁻/OH⁻ ratio, which is around 0.6 in solutions simulating the concrete pore solution.



C. Alonso analyzed the trials made by a number of researchers to calculate the different chloride thresholds to depassivate the reinforcing steel, as can be seen in Table 3.1. From the table it is obvious that there are large deviations in the chloride threshold between researchers. This lack in the calculations could be related to the existence of several parameters influencing the process, for instance, concrete mix proportions, moisture content, temperature, and other factors that were discussed before.

Another important reason is the different method for threshold identification for each researcher. *Hausmann & Gouda* consider that depassivation is produced when a certain shift in the corrosion potential is produced. *Thomas, Hope & Ip* use the visual inspection and identify depassivation with the appearance of rust spots on the steel surface. Some researchers like *Goni, Andrade, Lambert, Page* and others relate depassivation with a certain level in the corrosion current. A review of data collected from different authors made by *Glass and Buenfeld*, showed that the total chloride thresholds may vary from 0.15% to 2.5% by weight of cement.

In order to eliminate the variations in the authors' identification for chloride threshold, statistical analysis has been used. *Hausmann* in the sixties was the first that gave a statistical threshold distribution to predict rebar depassivation, using a $[Cl^-] / [OH^-]$ ratio and giving mean value of 0.6. Since then other authors have tried to make statistical approaches, giving mean values from 0.25% to 0.5% of total chloride by weight of cement, also fittings for a long normal distribution have been made giving values, with 95% probability for reinforcement depassivation, from 0.496% to 0.569% for free chlorides and from 0.623% to 0.771% for total chlorides, *M. Cruz (2008)*.

Finally and according to *M. Cruz*, a recent fitting made by an author using all chloride threshold values reported have allowed to defining histograms as those of Figs. 3.3 and 3.4 for free and total chlorides.



Table 3.1: Critical chloride levels required to initiate the corrosion of the reinforcing steel. Literature data wc: weight of cement, *Cement and Concrete Research 30 (2000)*

Reference	Environment	Values of intervals			Depassivation detection method
		Free Cl (% wc)	Total Cl (%wc)	Cl/OH	
Haussmann	Solution			0.6	Shift in corrosion potential, visual inspection
Gouda	Solution			0.35	Anodic polarization, shift in potentials and visual observation
Goni & Andrade	Solutions			0.25-0.8	Averaged corrosion rate
Gouda & Halaka	OPC		2.42		Anodic polarization
	BFSC		1.21		
Pettersson	Mortars			2.5-6.0	Corrosion rate
	80% RH		0.6-1.8	1.7-2.6	
	100% RH		0.5-1.7	1.7-2.6	
Andrade & Page	OPC			0.15-0.69	Corrosion rate
	BFSC			0.12-0.44	
Hansson & Sorensen	100% RH				Increase in current density
	50% RH		0.6-1.4		
Pettersson	Concrete			1.8-2.9	Corrosion rate
Lambert et al.	Concrete			3.00	Corrosion rate
Gouda & Halaka	OPC		3.04		Anodic polarization
	BFSC		1.01		
Gouda & Halaka	OPC		0.60		Anodic polarization
Kayyali & Haque	MS concrete	1.15			Assuming a threshold Cl/OH value of 0.6, calculation of free chlorides
	HS concrete	0.85			
	HSS	0.80			
	HSSFA	0.45			
Hussain et al.	2.43% C ₃ A concrete	0.14	0.35		Assuming a threshold Cl/OH value of 0.3
	7.59% C ₃ A concrete	0.17	0.62		
	14% C ₃ A concrete	0.22	1.00		
Schiessl & Breit	OPC		0.5-1		Macro-cells currents
	BFSC		1-1.5		
	FA		1-1.5		
Thomas et al.	Concrete		0.50		Visual observation + mass loss
Thomas	0% Fly ash		0.70		Mass loss
	15% Fly ash		0.65		
	30% Fly ash		0.50		
	50% Fly ash		0.20		
Hope & Ip	OPC		0.097-0.19		Corrosion rate, AC impedance, visual inspection, gravimetric mass loss

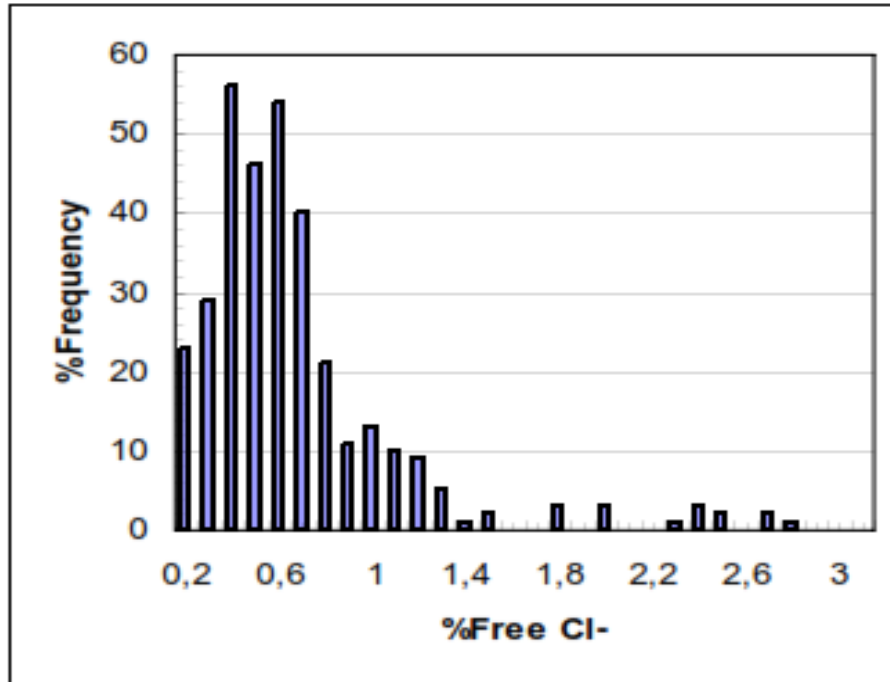


Fig. 3.3: Histogram of the free chloride threshold from the values published [Critical chloride content in reinforced concrete, 2008]

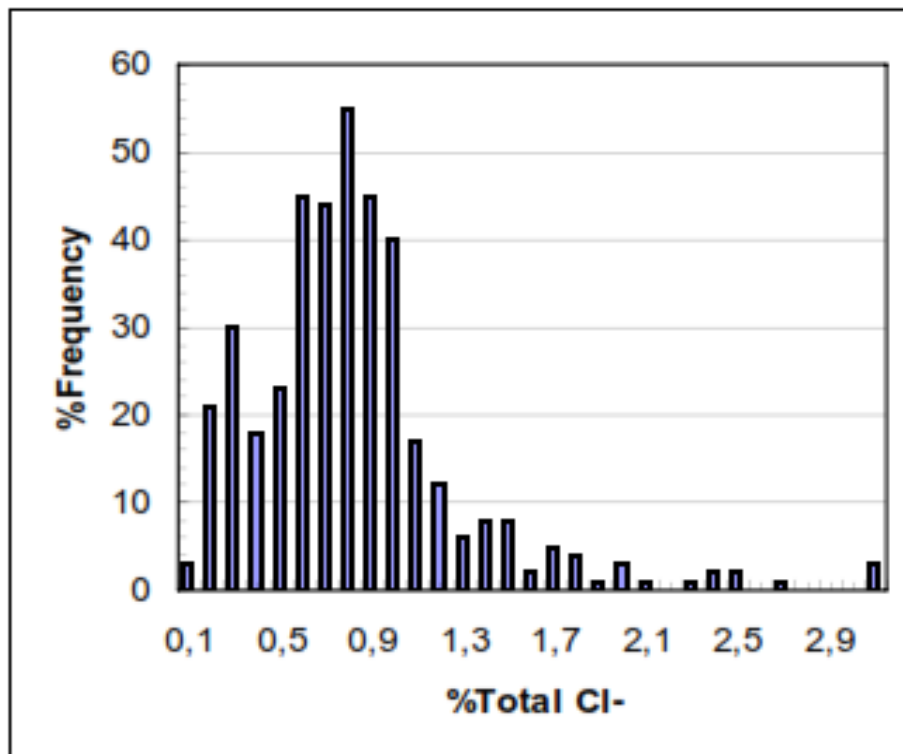


Fig. 3.4: Histogram of the total chloride threshold from the values published [Critical chloride content in reinforced concrete, 2008]



An experimental work was made by *Alonso et al.* to calculate the chloride threshold. Mortar specimens were used with two identical steel bars embedded in each specimen. In the first series, specimens were fabricated with smoothed bars, and in the second one, specimens with ribbed bars were fabricated. According to the results obtained from this experiment, the type of steel does not seem to influence significantly the threshold value although after depassivation. However, these results showed a bit higher susceptibility of the ribbed bars to be corroded in comparison to the smoothed ones.

3.6 Types of Corrosion

Several types of corrosion can occur which are identical in the chemical process, but differ in how and where they attack the metal. Table 3.2 shows the five major types of corrosion attack and their characteristics.

According to *Shreir L.L.*, a logical and scientific classification of corrosion processes is by no means simple, owing to the enormous variety of corrosive environments and the diversity of corrosion reactions, but the broad classification of corrosion reactions into 'wet' or 'dry' is now generally accepted, and the terms are in common use.

Shreir used the term 'wet corrosion' for all reactions in which an aqueous solution is involved in the reaction mechanism; and 'dry corrosion' for reactions that take place in the absence of water or an aqueous solution. Fig. 3.5 shows a schematic diagram for both dry and wet corrosion process.

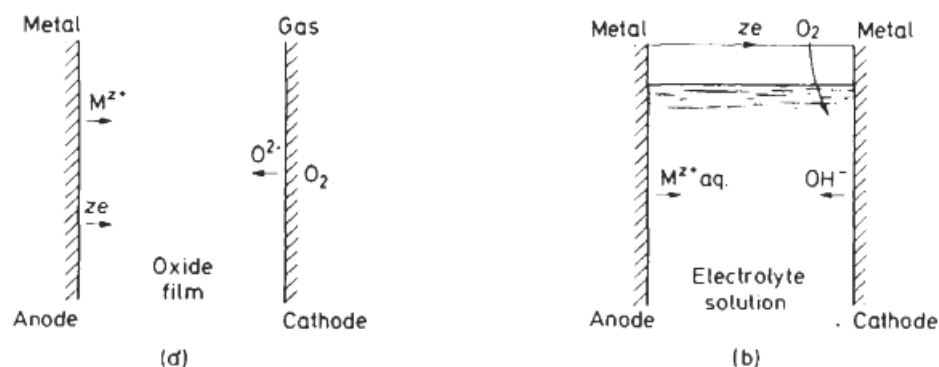


Fig. 3.5: Anodes and cathodes in corrosion processes. (a) Dry corrosion. (b) Wet corrosion.
 [Metal Environmental Reactions, 1994]



Table 3.2: Types of corrosion, *Metal Environmental Reactions, 1994*

Type	Characteristic	Examples
1. Uniform (or almost uniform)	All areas of metal corrode at the same rate.	Oxidation and tarnishing; active dissolution in acids; anodic oxidation and passivity; chemical and electrochemical polishing; atmospheric and immersed corrosion in certain cases.
2. Localized	Certain areas of the metal surface corrode at higher rates than others.	Crevice corrosion; deposit attack; bimetallic corrosion; weld decay.
3. Pitting	Highly localized attack at specific areas resulting in small pits that penetrate into the metal and may lead to perforation.	Pitting of passive metals such as the stainless steels, aluminum alloys, etc., in the presence of specific ions, e.g. Cl ⁻ ions.
4. Selective dissolution	One component of an alloy (usually the most active) is selectively removed from an alloy.	Dezincification; dealuminification; graphitization.
5. Conjoint action of corrosion and a mechanical factor	Localized attack or fracture due to the synergistic action of a mechanical factor and corrosion.	Erosion-corrosion, fretting corrosion, impingement attack, cavitation damage; stress corrosion cracking, hydrogen cracking, corrosion fatigue.



3.6.1 Dry Corrosion

As mentioned before dry reactions are those that can undergo in the absence of water or an aqueous solution. These are generally metal/gas or metal/vapor reactions. The oxidation and reduction processes take place between the metal and non-metal respectively. Compounds formed from these processes must occur at one and the same place at the metal/non-metal interface. Further reactions at the interface will lead to a thick film at the metal surface which acts as a barrier to the reactants and further interactions.

3.6.2 Wet Corrosion

In wet corrosion reaction; oxidation and reduction processes occur at different areas on the metal surfaces. First electrons transfer through the metal itself from anode (metal oxidized) to the cathode (electron acceptor reduced). The products of oxidation/reduction process may be solid products or hydrated ions (cations or anions) at the metal/solution interface. These products may be transported away from the interface by processes such as migration or diffusion. These products may undergo other chemical reactions with the solution resulting in the formation of a stable solid phase, but as this will form away from the interface it will not be a protective layer for the metal.

3.7 Corrosion Stages

Deterioration of reinforced concrete structures, especially in salt laden environments, due to steel bars corrosion go through four principle stages:

- 1- Chloride contamination and corrosion initiation.
- 2- Cracking.
- 3- Delamination.
- 4- Spalling.



Chloride contamination and corrosion initiation stage had been discussed before in the steel depassivation section. Cracking stage occurs when the corrosion-induced tensile stresses exceed the tensile strength of the concrete. Delamination occurs when the crack width increases and the bond strength between concrete and the embedded bars starts to deteriorate. Spalling happens when excessive loading causes the cracked delaminated portions to break away. In other words, it can be said that the corrosion cycle of steel begins with the rust expanding on the surface of the bar and causing cracking near the steel/concrete interface. As time marches on, the corrosion products build up and cause more extensive cracking until the concrete breaks away from the bar, eventually causing spalling. A simple model for the corrosion of steel in concrete introduced by *T. Paul* is shown in Fig. 3.6. This service life model for reinforced concrete structures has two stages – initiation and propagation. According to *T. Paul*, the initiation time is the length of time until depassivation of the steel reinforcing bars and the initiation of corrosion has occurred. After that the corrosion started and its rate may increase or decrease according to several important factors as: chloride profile, cover depth, carbonation depth, concrete resistivity, and the environment. At some point, cracking and spalling occur and the structure is either rehabilitated or has reached the end of its service life and replaced.

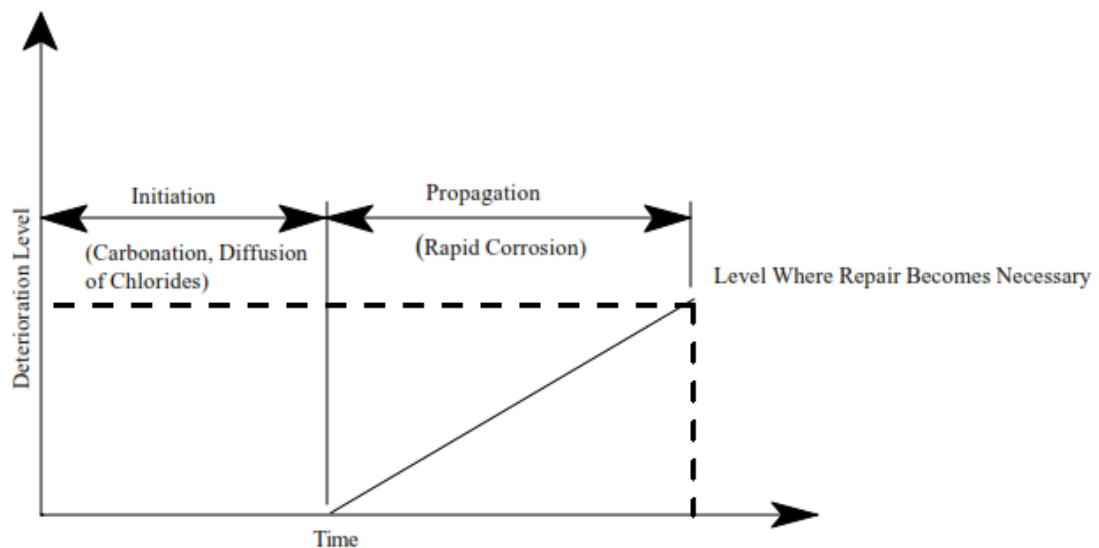


Fig. 3.6: Simple Deterioration model, corrosion of steel in concrete
[*Materials and Methods for Corrosion Control, 2000*]



3.8 Factors Affecting Corrosion and its Rate

Rate of concrete reinforcement corrosion can be affected by many factors. These factors can be classified into two principle categories: Factors related to the concrete itself, and others related to the surrounding environment.

3.8.1 Factors Related to Concrete

Concrete is a composite material made of aggregates and the reaction product of the cement and the mixing water. The structure and composition of the cement paste determines the durability and the long term performance of concrete, and also determines the efficiency of the protection that concrete provides to the embedded steel. Concrete has three main transport properties, permeability, diffusivity and sorptivity.

3.8.1.1 Permeability

Permeability is the rate of flow of a fluid under pressure in a porous material. This means that this property is highly affected by the porosity and the pore structure of the concrete. Porosity of a material is defined as the ratio of the volume of all pores in a material to the whole volume. The distribution of the pores plays a big role in the flow of fluids within the concrete. The connectivity can help the flow of liquid through the concrete. If the pores are connected, fluids are allowed to move in many paths of flow, but if they are disconnected the fluid is trapped and cannot move on, *Z. Aldulaymi, (2007)*.

The cement paste formed by the hydration reactions always contains interconnected pores of different sizes, as shown in Fig. 3.7. *L. Bertolini* divided these pores into macro-pores, capillary pores and gel pores. The interlayer spacing within gel pores (C-S-H) has a volume equal to about 28% of the gel and dimensions ranging from a few fractions of a nm to several nm. These don't have a remarkable effect on the concrete durability and its protection of the reinforcement, since they are too small to allow significant transport of aggressive species. The capillary pores are the voids



not filled by the solid products of hydration of hardened cement paste. They have dimensions of 10 to 50 nm if the cement paste is well hydrated and produced using low water/cement ratios (w/c), but can reach up to 3-5 μm if the concrete is made using high w/c ratios or it is not well hydrated. Also *L. Bertolini* defined another type of large pores resulting from the air entrapped during mixing and not removed by compaction of fresh concrete. These pores may reach few mms in size. Special admixtures like air entraining admixtures which are used to produce light weight concrete result in the formation of air bubbles with diameters of about 0.05-0.2 mm.

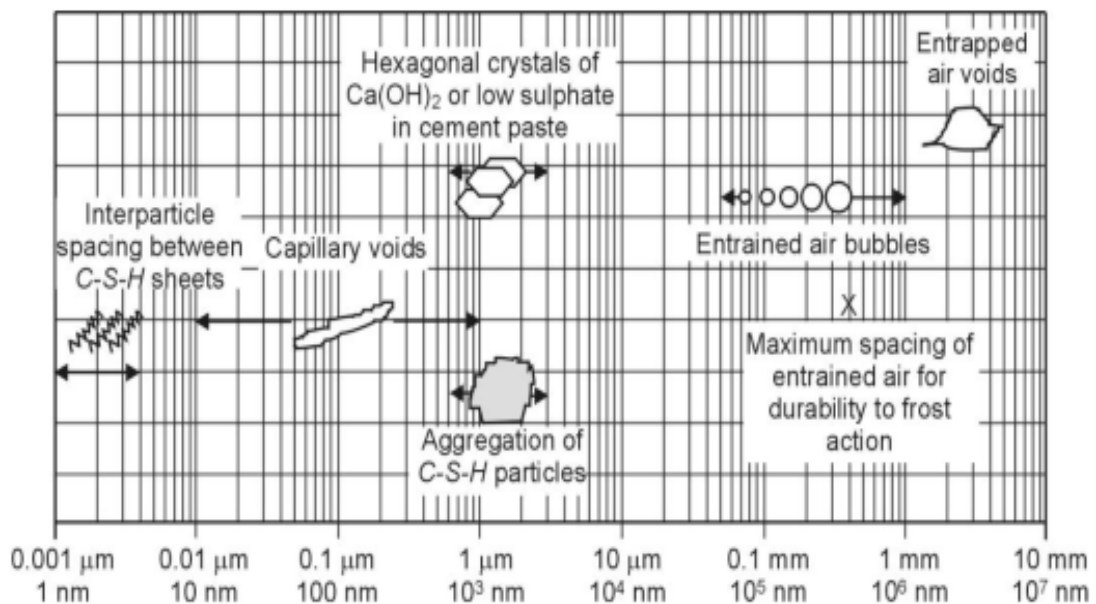


Fig. 3.7: Dimensional range of solids and pores in hydrated cement paste
 [Corrosion of steel in concrete, 2004]

3.8.1.2 Diffusivity

Diffusivity is defined as the spread of fluids in concrete under a concentration gradient. For this to occur the concrete must have a continuous liquid phase and there must be a chloride ion concentration gradient, *Stanish et al. (1997)*. Chloride ion diffuses only when dissolved in water, and the diffusion is more effective when the pore system is fully saturated, *Bertolini (2004)*.



3.8.1.3 Sorptivity

Bentz defined sorptivity as the ingress of water into non-saturated structure driven by capillary forces. This means that porous concrete absorbs more water and faster than a dense concrete. In 2004, *Bertolini* derived an empirical equation from the observation of experimental data to estimate concrete sorptivity. According to the author, this equation is only correct for very porous materials or in the early stages of capillary action.

$$i = S(t)^{1/2} \quad 3 - 4$$

where:

i: liquid absorbed per unit of surface (gm/m^2 for mass or m^3/m^2 for volume)

t: time (sec)

S: concrete sorptivity ($gm/m^2 \cdot s^{1/2}$) for mass change or ($m/s^{1/2}$) for absorbed volume

The values of concrete sorptivity depend on a variety of factors, but the main factor is the degree of drying to which the samples have been subjected, *Z. Aldulaymi* (2007).

3.8.1.4 Water/cement Ratio and Curing

There are other factors that are related to the concrete itself and its manufacturing like the chosen water/cement ratio and the concrete cover thickness. Water plays an important role in the hydration of cement paste, since it is the main factor in converting the dry cement powder into the hydrated products as shown in Fig. 3.8. It had been said that the initial volume of a mixture of cement powder and water doesn't change after hydration, where the sum of volumes of mixed water (V_w) and cement (V_c) is equal to the volume of the hardening products. This volume consists of the sum of the volume of un-hydrated cement (V_{uc}), the hydrated cement ($V_p + V_{gw}$) and the capillary pores that are filled by water (V_{cw}) or by air (V_{ec}). The volume of the products of hydration can be assumed to be roughly double that of the cement; hence during hydration these products fill the space previously occupied by the cement that has hydrated and part of the surrounding space initially occupied by water as shown in Fig. 3.9.

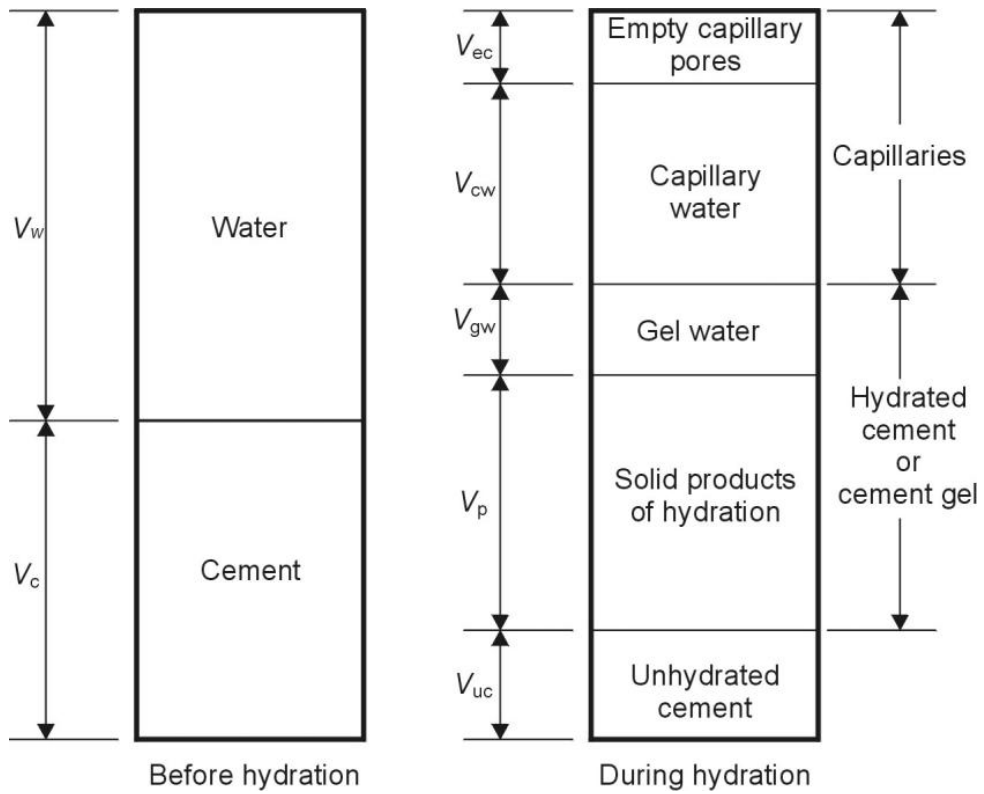


Fig. 3.8: Schematic Representation of the Volumetric Proportions in Cement Paste Before & During Hydration
 [Neville and Brooks]

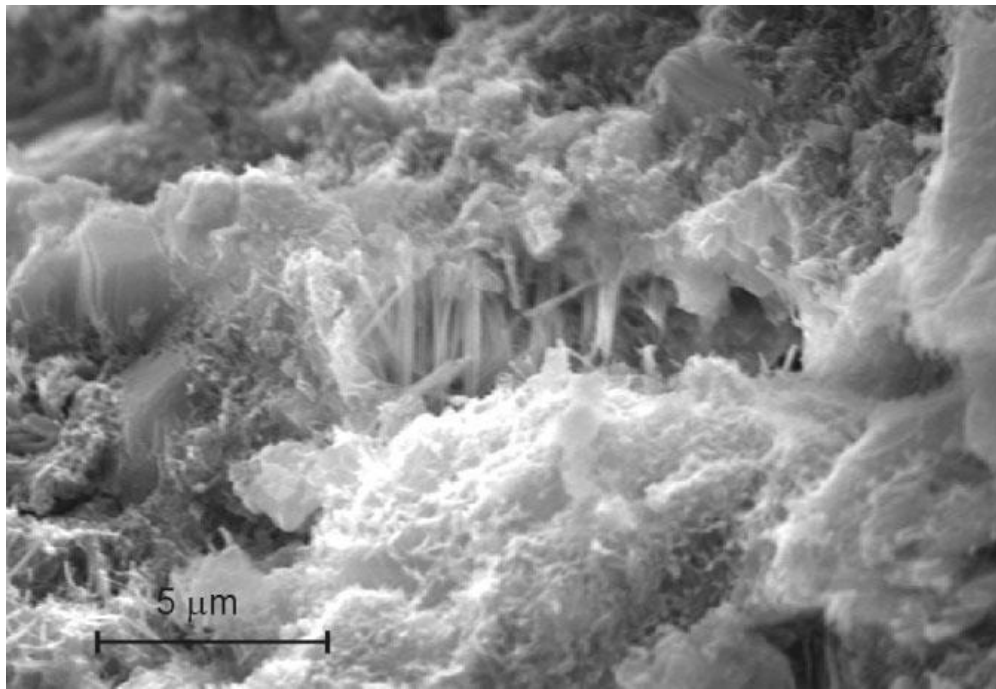


Fig. 3.9: Example of Micro-structure of Hydrated Cement Paste (scanning electron microscope)
 [Corrosion of steel in concrete, 2004]



Therefore, curing of cement after setting is a very important issue. This gives chances for the hydration process to proceed and this will result in decreasing the volume of the capillary pores. Volume of pores will reach a minimum when the hydration of cement has completed. Fig. 3.10 shows that the pore-size distribution depends on w/c ratio and curing time. It is obvious that as the w/c ratio decreases, or as the curing time increases, the reduction of porosity is mainly due to the reduction in pores of larger dimensions that have been filled or have been connected only by C-S-H gel pores, *Bertolini*.

Powers proposed a formula for estimating the volume of capillary pores (in litres per kg of cement). His assumptions were that the volume of capillary pores (V_{cp}) in the cement paste increases with the amount of water used in the paste and thus with the water/cement ratio (w/c) and decreases with the degree of hydration (h), i.e. the fraction of hydrated cement.

$$V_{cp} = (w/c - 0.36h) \quad 3 - 5$$

The Egyptian Code of Practice gives maximum limits for the water/cement ratio to ensure good durability for concrete and efficient protection to the embedded steel bars. The code limits are (w/c= 0.50) for concrete secured from any harmful environmental impacts and (w/c=0.40) for concrete that is surrounded by harmful environmental effects and is subjected to cycles of freezing and thawing.

3.8.1.5 Concrete Cover Thickness

The thickness of concrete cover is an important factor in delaying the corrosion initiation. The larger the concrete cover the longer the time required for the chloride to reach the reinforcing steel surface. This doesn't mean that thick cover is an optimum solution to delay corrosion initiation. Any code has a minimum and maximum limit for the concrete cover thickness. Typically, the concrete cover should not exceed (80 – 100) mm. Thick concrete cover may have an adverse effect if not associated with steel due to shrinkage cracks and thermal stresses. Small thickness of concrete cover



should also be avoided because cracks for any reason could result in rapid transportation of chloride ions to the surface of the reinforcing steel.

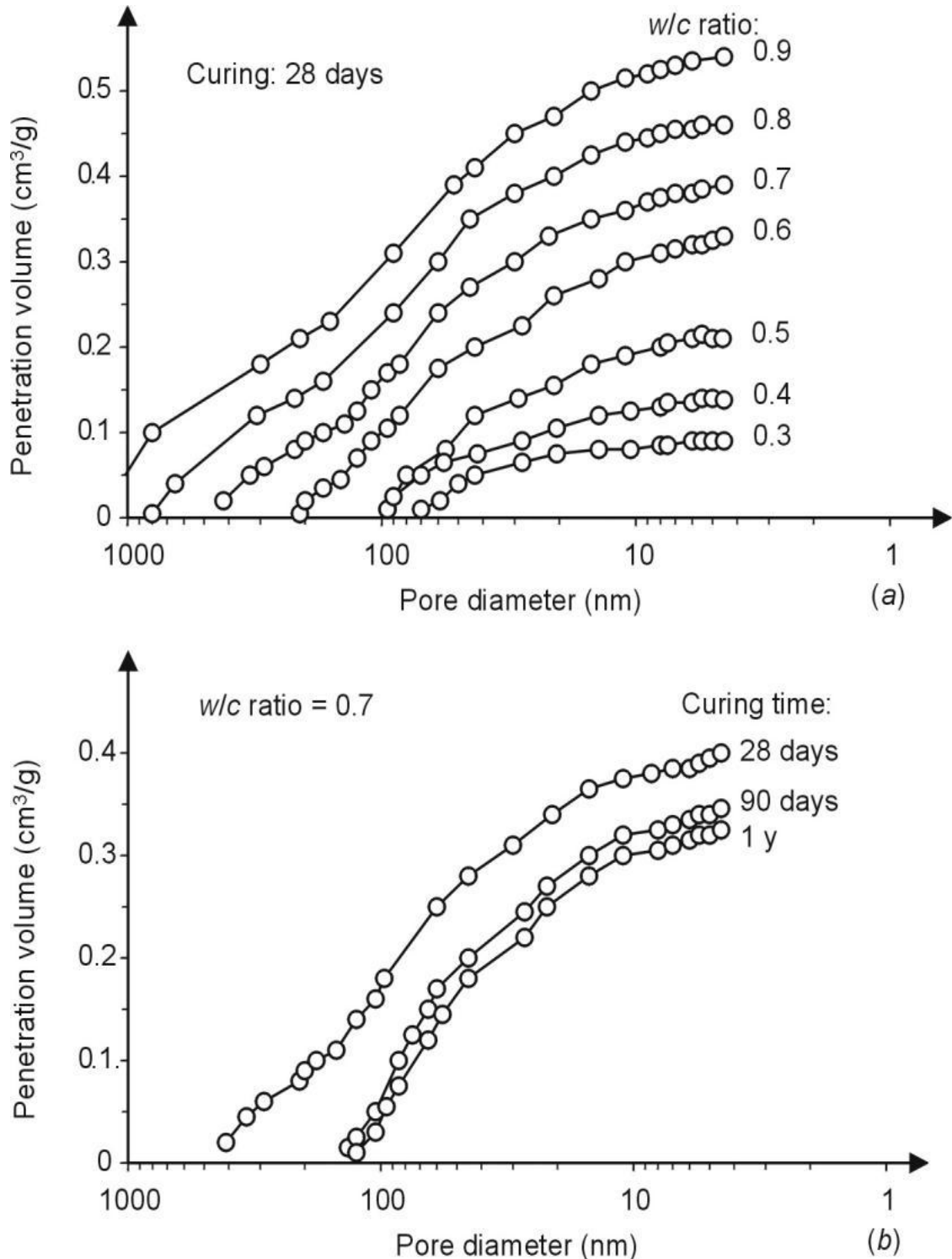


Fig. 3.10: Influence of the Water/cement Ratio and Curing on the Distribution of Pore Size in Hydrated Cement Pastes

[Corrosion of steel in concrete, 2004]



The low permeability and the concrete cover thickness can compensate each other, *Neville (1995)*. For this reason standards often specify a combination of cover thickness and concrete strength, such that a higher concrete strength and a lower concrete cover and vice versa.

Bertolini summarizes the transport processes in concrete as shown in Fig. 3.11, showing the factors involved in each process and the way of transport.

Fig. 3.12 shows two graphical representations made by *Bertolini* which show the relation between capillary pores, concrete strength, permeability of cement paste, water/cement ratio, and degree of hydration. From the graphs it is shown that the decrease in capillary porosity increases the mechanical strength of cement paste and reduces the permeability of the hydrated cement paste.

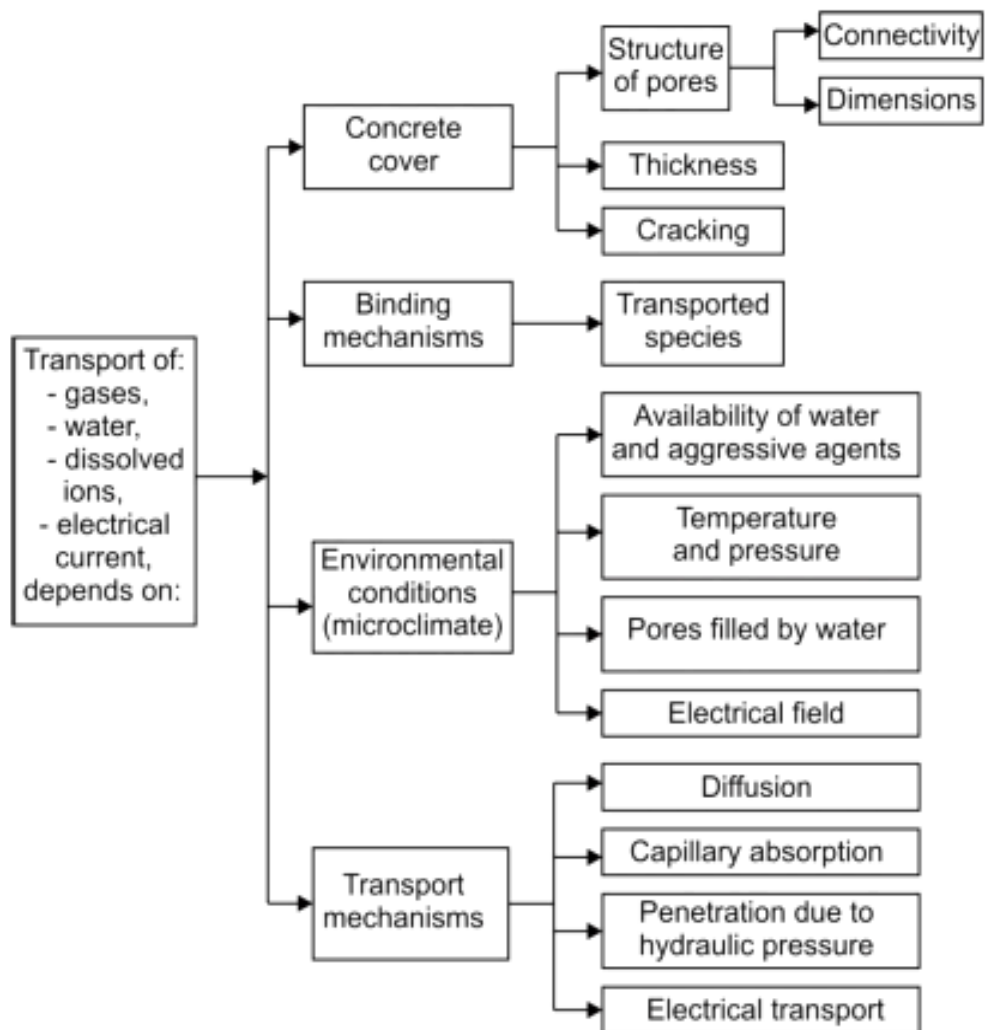


Fig. 3.11: Principle Factors Involved in the Transport Processes in Concrete, Essential in the Phenomenon of Corrosion
 [*Corrosion of steel in concrete, 2004*]



3.8.2 Factors Related to the Surrounding Environment

This research deals with structures near sea side, therefore let's discuss the factors related to marine environment which is a good example of sea side reinforced concrete structures. Considerable advances have been made in concrete technology in recent years and all these will assist in providing the right materials for specific marine applications in the future.

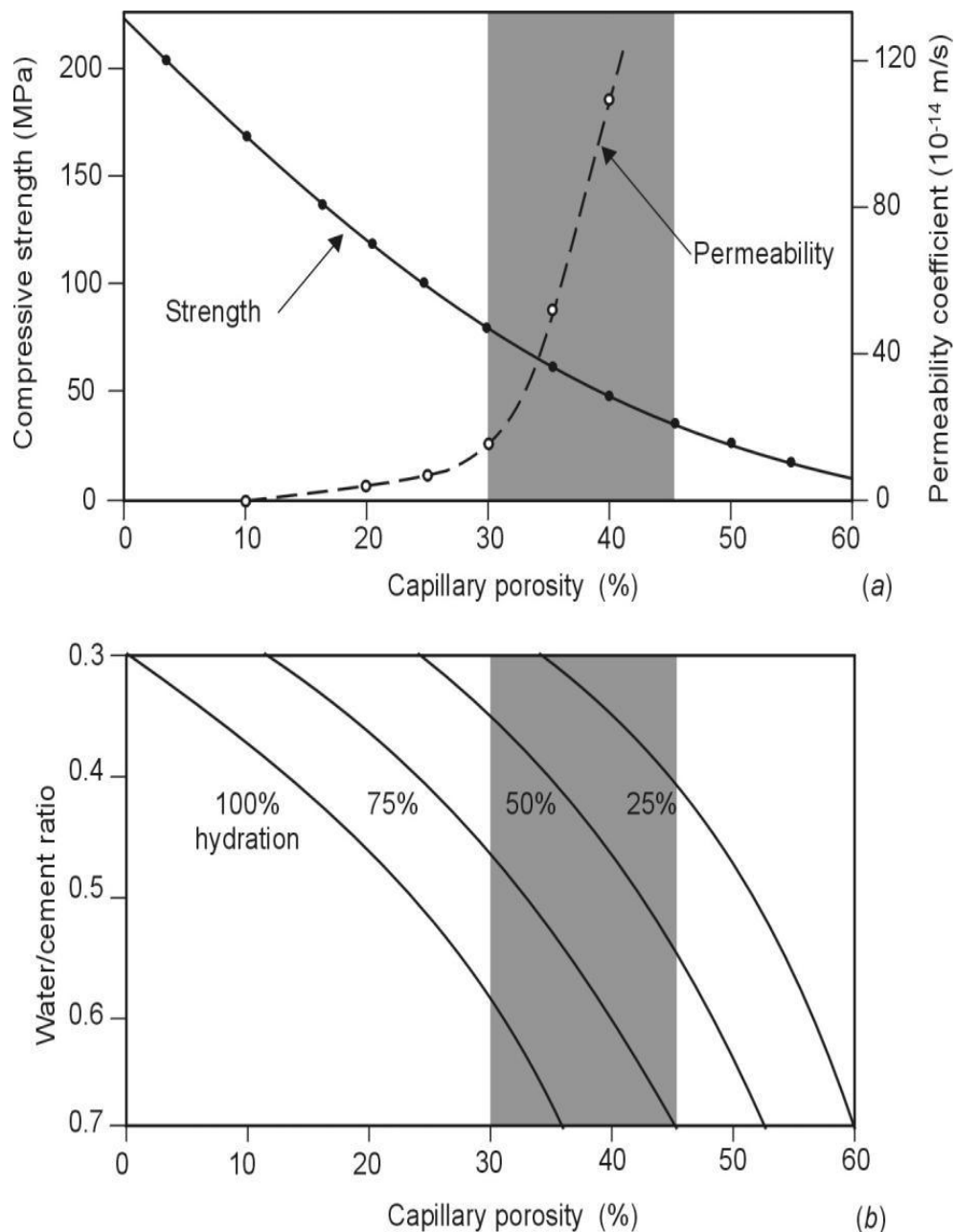


Fig. 3.12: a) Influence of capillary porosity on strength and permeability of cement paste. b) Capillary porosity derived from a combination of water/cement ratio and degree of hydration, Powers equation [Corrosion of steel in concrete, 2004]



Concrete in a marine environment undergoes different deterioration processes depending on the position of the structure. Some structures may be totally submerged, others may be in the atmospheric zone and others are located in between where they are subjected to water and air. Fig. 3.13 shows a schematic diagram by *Mehta* showing the different zones of marine environment.

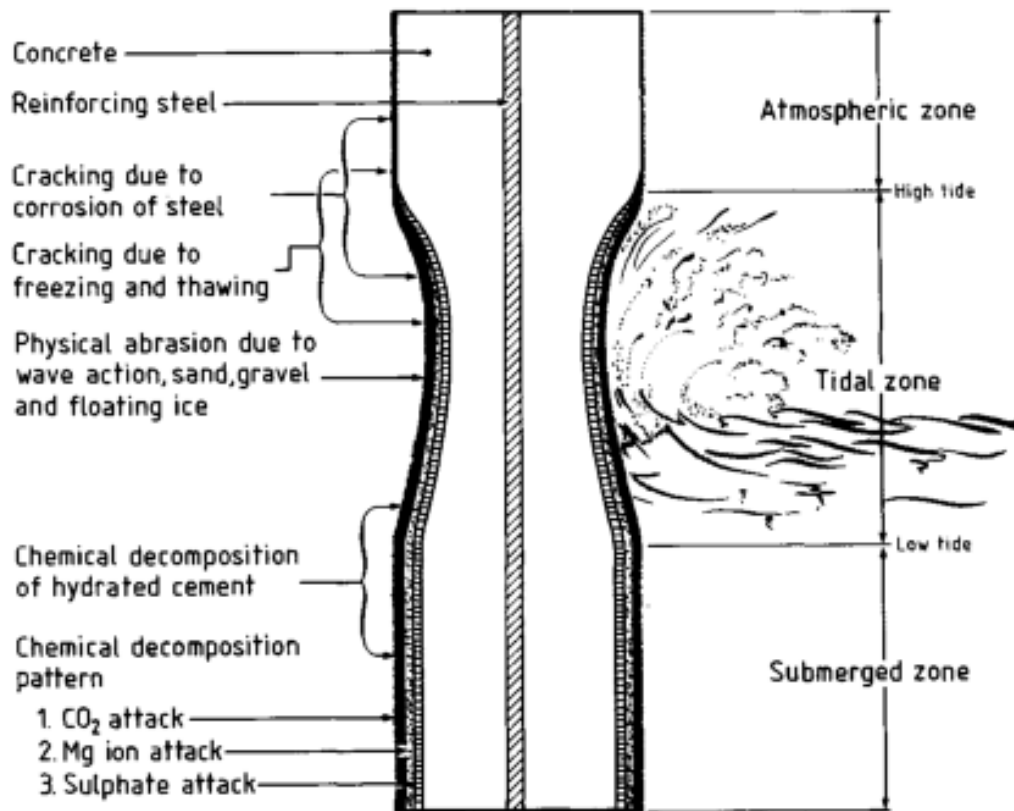


Fig. 3.13: Marine Exposure Zones of Concrete Structures
[Durability of concrete in the marine environment]

3.8.2.1 Atmospheric Zone

The concrete is exposed to salt spray and cycles of wetting and drying. This zone is most prone to chloride-induced reinforcement corrosion resulting in cracking and spalling of the concrete cover. This mainly occurs on the frontage of buildings facing the sea like those buildings located in Alexandria, Egypt (Fig. 3.14).



Fig. 3.14: Concrete cover spalling
[El-Montaza, Alexandria, Egypt]

3.8.2.2 Tidal Zone

This is the zone between the low and high tide levels. The concrete undergoes wet and dry cycles of sea water exposure. Mechanical action of waves carrying sand and gravel causing abrasion, results in loss of the concrete cover thickness which increases the chances for steel bars corrosion to a large extent. Chemical decomposition of Portland cement hydrate is also likely in this zone, (Fig. 3.15).



Fig. 3.15: Abrasion & cement decomposition in tidal zone
[El-Montaza, Alexandria, Egypt]



3.8.2.3 Submerged Zone

It is the zone totally covered with sea water. This zone is subjected to chemical attack by the salts in sea water on the products of hydration of Portland cement. Sea water in this zone lacks dissolved oxygen to fuel corrosion of reinforcement. The hydrostatic pressure caused by the depth of sea water is likely to result in rapid diffusion of chloride into concrete, *P. S. Mangat*. The availability of oxygen is a function of its rate of diffusion through the concrete. When concrete is totally submerged, the diffusion rate of oxygen is slowed because the oxygen must diffuse through the pore water. When the concrete is dry, the oxygen can freely move through pores, *T. Paul*.

Table 3.3 summarizes the primary chloride transport mechanisms applicable to structures in various exposure conditions.

Table 3.3: Chloride transport mechanisms, *Chloride Resistance of Concrete, 2009*

Exposure	Example of structures	Primary chloride transport mechanism
Submerged	Substructures below low tide	Diffusion.
	Basement exterior walls or transport tunnel liners below low tide. Liquid containing structures.	Permeation, diffusion and possibly Wick's action.
Tidal	Substructures and superstructures in the tidal zone.	Capillary absorption and diffusion.
Splash and spray	Superstructures about high tide in the open sea.	Capillary absorption and diffusion. (Also carbonation)
Coastal	Land based structures in coastal area or superstructures above high tide in river estuary or body of water in coastal area	Capillary absorption. (Also carbonation)

3.9 Chloride Resistance of Concrete

As mentioned before; concrete provides physical and chemical protection to the reinforcing steel bars from penetrating chlorides which may cause steel depassivation leading to increased risk of steel corrosion. The concrete resistance to chlorides